

Optimized Unrestricted Kohn–Sham Potentials from *Ab Initio* Spin Densities

Katharina Boguslawski^a, Christoph R. Jacob^{b,1}, and Markus Reiher^{a,2}

^aETH Zurich, Laboratorium für Physikalische Chemie, Wolfgang-Pauli-Str. 10,
CH-8093 Zurich, Switzerland

^bKarlsruhe Institute of Technology (KIT), Center for Functional Nanostructures,
Wolfgang-Gaede-Straße 1a, 76131 Karlsruhe, Germany

Abstract

The reconstruction of the exchange–correlation potential from accurate *ab initio* electron densities can provide insights into the limitations of the currently available approximate functionals and provide guidance for devising improved approximations for density-functional theory (DFT). For open-shell systems, the spin density is introduced as an additional fundamental variable in Spin-DFT. Here, we consider the reconstruction of the corresponding unrestricted Kohn–Sham potentials from accurate *ab initio* spin densities. In particular, we investigate whether it is possible to reconstruct the spin exchange–correlation potential, which determines the spin density in spin-unrestricted Kohn–Sham-DFT, despite the numerical difficulties inherent to the optimization of potentials with finite orbital basis sets. We find that the recently developed scheme for unambiguously singling out an optimal optimized potential [*J. Chem. Phys.*, **135**, 244102 (2011)] can provide such spin potentials accurately. This is demonstrated for two test cases, the lithium atom and the dioxygen molecule, and target (spin) densities from Full-CI and CASSCF calculations, respectively.

Date: November 21, 2012

Status: submitted to *J. Chem. Phys.*

¹Corresponding Author; E-Mail: christoph.jacob@kit.edu

²Corresponding Author; E-Mail: markus.reiher@phys.chem.ethz.ch

1 Introduction

Density-functional theory (DFT) within the Kohn–Sham (KS) framework [1, 2] represents one of the most frequently applied quantum-chemical methods for electronic structure calculations and for the determination of molecular properties. Its success relies on the accuracy of existing approximations to the exchange–correlation energy functional $E_{xc}[\rho]$ and to the exchange–correlation potential $v_{xc}[\rho] = \delta E_{xc}[\rho]/\delta\rho$, i.e., the functional derivative of $E_{xc}[\rho]$ with respect to the electron density $\rho(\mathbf{r})$ [3]. However, for open-shell systems, in particular for transition metal complexes, the existing approximations have a number of severe shortcomings [4–6], for instance for the prediction of the energy differences between different spin states [7–11] and of spin-density distributions [12–15].

While the universal functionals $E_{xc}[\rho]$ and $v_{xc}[\rho]$ are unknown, there exists a numerical recipe for obtaining the exact exchange–correlation potential $v_{xc}[\rho_0]$ corresponding to the ground-state electron density ρ_0 of arbitrary atomic and molecular systems. First, this ground-state electron density ρ_0 can be calculated accurately — and in principle exactly — using wave-function based *ab initio* calculations. Second, the Kohn–Sham potential $v_s[\rho_0]$ that yields the density ρ_0 in a noninteracting system can be reconstructed. Finally, by subtracting the known nuclear and Coulomb potentials from this reconstructed potential, the exchange–correlation potential $v_{xc}[\rho_0]$ can be obtained. Such reconstructed ground-state exchange–correlation potentials can provide guidance for the construction of approximate exchange–correlation potentials [16–19] and energy functionals [20–22].

The key step in the above recipe is the reconstruction of the potential $v_s[\rho_0]$ from the target density ρ_0 . This step corresponds to an inverse problem in quantum chemistry [23], i.e., the potential is sought which generates a given target density in a noninteracting reference system. This potential reconstruction is also essential for quantum-chemical subsystem and embedding methods (for a review, see Ref. [24]), in which it can be used to avoid the need for approximating the nonadditive kinetic-energy [25–29], or for developing better approxi-

mations for this part of the embedding potential [30–33].

The inverse problem of reconstructing the noninteracting local potential yielding a given target density is equivalent to evaluating the functional derivative of the noninteracting kinetic-energy functional $T_s[\rho]$ [34,35], which is an implicit functional of the electron density. For evaluating such functional derivatives of implicit functionals, the optimized effective potential (OEP) method can be employed, which tackles the inverse problem by minimizing the implicit functional with respect to the local potential [36–38], possibly subject to additional constraints [39]. Thus, the reconstruction of local potentials is a special case of the more general problem of evaluating the functional derivative of implicit density functionals.

For applying OEP methods to many-electron systems and large molecules, both the orbitals and the local potential have to be expanded in finite basis sets. The introduction of a finite orbital basis set, however, turns the OEP method into an ill-posed problem and the solution becomes non-unique [40]. The ill-posed nature is common to many inverse problems and makes the inverse mapping from an electron density to a local potential unstable and sensitive to optimization parameters. Furthermore, these drawbacks result in unphysical potentials, which can contain large oscillations affecting orbital energies and derived properties [40,41].

To allow for a routine application of the OEP method in quantum chemistry, approaches to regularize the OEP solutions have been proposed. One approach developed by Heßelmann *et al.* is based on explicitly constructing an orbital basis set that is balanced with respect to the basis set employed for expanding the potential [42], whereas the orbital basis set is balanced implicitly in the approach of Kollmar and Filatov [43,44]. However, these methods require very large orbital basis sets, which hampers their application to larger molecular systems. A different approach was developed by Yang and co-workers [41,45], who introduced a regularization parameter in the energy functional to make the resulting optimized potentials as smooth as possible. Recently, an approach which yields unambiguous potentials for any combination of orbital and potential basis sets and that provides high-quality poten-

tials already with small orbital basis sets was suggested by one of us [46]. It is based on the condition that the optimal reconstructed potential should yield the target density when extending the orbital basis set.

So far, OEP methods for reconstruction the exchange–correlation potential from accurate *ab initio* densities have mainly been applied to closed-shell systems, i.e., to the total electron density as target only (for exceptions, see, Refs. [31, 47]). For open-shell systems, one commonly employs an unrestricted KS-DFT formalism [1, 48, 49], in which the spin density $Q(\mathbf{r}) = \rho^\alpha(\mathbf{r}) - \rho^\beta(\mathbf{r})$ is used as an additional fundamental variable. This leads to separate KS equations for α - and β -electrons containing different exchange–correlation potentials $v_{\text{xc}}^\alpha[\rho, Q] = \delta E_{\text{xc}}[\rho, Q]/\delta\rho_\alpha$ and $v_{\text{xc}}^\beta[\rho, Q] = \delta E_{\text{xc}}[\rho, Q]/\delta\rho_\beta$, i.e., the α - and β -electron densities ρ^α and ρ^β , respectively, are determined separately. In such a formalism, the exact spin-resolved exchange–correlation functional would yield — in addition to the exact total electron density — also the exact spin density [49–51]. While the total electron density is determined by the total exchange–correlation potential $v_{\text{xc}}^{\text{tot}}[\rho, Q] = \frac{1}{2}(v_{\text{xc}}^\alpha[\rho, Q] + v_{\text{xc}}^\beta[\rho, Q])$, the spin density in unrestricted KS-DFT is determined by the spin exchange–correlation potential $v_{\text{xc}}^{\text{spin}}[\rho, Q] = \frac{1}{2}(v_{\text{xc}}^\alpha[\rho, Q] - v_{\text{xc}}^\beta[\rho, Q])$ [49]. Thus, for improving the spin-density dependence of approximate exchange–correlation potentials, it would be desirable to be able to reconstruct this spin exchange–correlation potential $v_{\text{xc}}^{\text{spin}}[\rho_0, Q_0]$ from accurate *ab initio* total and spin densities.

When using finite orbital basis sets, such a reconstruction of $v_{\text{xc}}^{\text{spin}}[\rho_0, Q_0]$ is particularly challenging, as it will be more sensitive to numerical errors than for the total or the individual α - and β -electron potentials. Here, we extend the unambiguous potential reconstruction developed in Ref. [46] to the spin-unrestricted cases and apply it to the reconstruction of the spin exchange–correlation potential from accurate *ab initio* (spin) densities. This requires some numerical enhancements of our implementation prompted by the use of Gaussian-type orbitals (GTOs) for expanding the orbitals in such wave-function based calculations. Moreover, the quality of the reconstructed spin potentials needs to be assessed carefully, if

possible by comparison to reference potentials reconstructed in fully numerical calculations.

This work is organized as follows. Section 2 briefly reviews the potential reconstruction algorithm and outlines its extension to the spin-unrestricted case. In Section 3, the computational methodology and extensions of our implementation are described. Subsequently, we study the reconstructed exchange–correlation potentials for two test cases, the lithium atom and the O₂ molecule, in Section 4. Here, target densities from both KS-DFT calculations and from accurate wave-function based *ab initio* calculations (Full-CI and CASSCF) are employed. Finally, our conclusions are summarized in Section 5.

2 Theoretical Background

2.1 Determining Optimized Unrestricted Kohn–Sham Potentials

Within spin-unrestricted KS-DFT, the wavefunction of the KS reference system is given by a (spin-unrestricted) N -electron Slater determinant, which is constructed from $N = N^\alpha + N^\beta$ orthonormal one-particle functions $\{\phi_i^\sigma(\mathbf{r})\sigma(s), \sigma = \alpha, \beta\}$. The corresponding spatial orbitals $\phi_i^\sigma(\mathbf{r})$ can then be determined by solving two separate sets of one-electron equations [49],

$$\left[-\frac{1}{2}\Delta + v_s^\alpha(\mathbf{r})\right] \phi_i^\alpha(\mathbf{r}) = \varepsilon_i^\alpha \phi_i^\alpha(\mathbf{r}) \quad \text{and} \quad \left[-\frac{1}{2}\Delta + v_s^\beta(\mathbf{r})\right] \phi_i^\beta(\mathbf{r}) = \varepsilon_i^\beta \phi_i^\beta(\mathbf{r}), \quad (1)$$

and the α - and β -electron densities are given by

$$\rho^\alpha(\mathbf{r}) = \sum_i^{N^\alpha} |\phi_i^\alpha(\mathbf{r})|^2 \quad \text{and} \quad \rho^\beta(\mathbf{r}) = \sum_i^{N^\beta} |\phi_i^\beta(\mathbf{r})|^2. \quad (2)$$

Here, we consider the inverse problem of determining the spin-resolved KS potential [i.e., the local potentials $v_s^\alpha(\mathbf{r})$ and $v_s^\beta(\mathbf{r})$] from given α - and β -electron target densities, $\rho_0^\alpha(\mathbf{r})$ and $\rho_0^\beta(\mathbf{r})$, that is, we require

$$\rho^\alpha(\mathbf{r}) = \rho_0^\alpha(\mathbf{r}) \quad \text{and} \quad \rho^\beta(\mathbf{r}) = \rho_0^\beta(\mathbf{r}). \quad (3)$$

An alternative way of expressing this problem is to consider the total and spin densities [49],

$$\rho_0(\mathbf{r}) = \rho^\alpha(\mathbf{r}) + \rho^\beta(\mathbf{r}) \quad \text{and} \quad Q(\mathbf{r}) = \rho^\alpha(\mathbf{r}) - \rho^\beta(\mathbf{r}) \quad (4)$$

as target, and to regard the total and spin potentials [49],

$$v_s^{\text{tot}}(\mathbf{r}) = \frac{1}{2} (v_s^\alpha(\mathbf{r}) + v_s^\beta(\mathbf{r})) \quad \text{and} \quad v_s^{\text{spin}}(\mathbf{r}) = \frac{1}{2} (v_s^\alpha(\mathbf{r}) - v_s^\beta(\mathbf{r})) \quad (5)$$

as the quantities that are sought. Here, $v_s^{\text{tot}}(\mathbf{r})$ is the potential determining the total electron density, whereas $v_s^{\text{spin}}(\mathbf{r})$ determines the spin density. Therefore, this representation will be particularly useful for understanding the dependence the exchange–correlation potential on the spin density $Q(\mathbf{r})$ and to identify the reason for the failure of approximate exchange–correlation functionals to describe the spin density correctly in some cases [15].

In principle, any method applicable for reconstructing the KS-potential in closed-shell systems could be adapted to the spin-unrestricted case by applying it separately to the α - and β -electron densities. However, already the closed-shell case poses many numerical difficulties, and achieving uniform accuracy for the α - and β -spin potentials, as it is required for obtaining $v_s^{\text{spin}}(\mathbf{r})$ accurately, turns out to be a challenging task.

The conceptually simplest approach for determining the local potential yielding a given target density is to represent the potential numerically on a grid and to determine it iteratively. Several methods working along these lines have been developed over the past decades [16, 52–55]. Generally, these methods calculate the density from some trial potential and then update the potential by comparing the density to the target density. If the density is too large at a grid point, the potential is made more repulsive at this point. Conversely, if the density is too small, the potential is made more attractive. This process is repeated iteratively until the target density is obtained. Different numerical potential reconstruction methods differ in the way in which the potential is updated in each iteration [16, 54, 55]. The only exception is the method of Zhao–Morrison–Parr (ZMP) [53], which uses a conceptually different approach.

However, such numerical methods also require that the KS equations [Eq. (1)] are solved numerically on the same grid. Therefore, their application has mainly been limited to (closed-shell) atoms and, in some cases, (closed-shell) diatomic molecules [56, 57]. Here, we will employ such a fully numerical scheme to obtain accurate reference potentials for atoms. For determining optimized KS potentials in general molecular systems, both the orbitals and the potential are usually expanded in a basis set [37, 39]. However, as will be discussed below, with finite orbital basis sets the potential reconstruction turns into an ill-posed problem, in which the resulting potential is not unique [40, 41, 58].

To overcome the resulting numerical difficulties, we will apply the recently developed unambiguous optimization method [46] and generalize it to unrestricted KS potentials. This scheme is based on a two-step procedure, in which one first determines a non-unique potential using a direct optimization in a finite basis set. Subsequently, an unambiguous optimized potential is singled out by means of a suitable criterion.

2.2 Direct Optimization of Unrestricted Kohn–Sham Potentials

In the first step, two non-unique local potentials $v_s^\alpha(\mathbf{r})$ and $v_s^\beta(\mathbf{r})$ yielding the target α - and β -electron densities $\rho_0^\alpha(\mathbf{r})$ and $\rho_0^\beta(\mathbf{r})$, respectively, in a given finite basis set have to be determined. To this end, we apply the direct optimization method by Wu and Yang [39] and extend it to the spin-unrestricted case.

The KS kinetic energy for any pair of α - and β -electron densities $\rho_0^\alpha, \rho_0^\beta$ is defined as [1, 59]

$$T_s[\rho_0^\alpha, \rho_0^\beta] = \min_{\Psi_s \rightarrow \rho_0^\alpha, \rho_0^\beta} \langle \Psi_s | \hat{T} | \Psi_s \rangle = \frac{1}{2} T_s[2\rho_0^\alpha] + \frac{1}{2} T_s[2\rho_0^\beta] \quad (6)$$

where $\hat{T} = -\Delta/2$ is the kinetic-energy operator and where the minimization includes all wavefunctions Ψ_s corresponding to a spin-unrestricted N -electron Slater determinant with α - and β -electron densities $\rho^\alpha(\mathbf{r})$ and $\rho^\beta(\mathbf{r})$. Hence, $T_s[\rho_0^\alpha, \rho_0^\beta]$ corresponds to the minimum kinetic energy of an unrestricted KS wave function Ψ_s under the constraint that its α - and

β -electron densities equal the target densities [60,61].

The constraint minimization problem of Eq. (6) can be reduced to two separate problems for $2\rho^\alpha$ and $2\rho^\beta$, respectively, which results in two Lagrangian functionals, $W^\alpha[\rho^\alpha(\mathbf{r})]$ and $W^\beta[\rho^\beta(\mathbf{r})]$, subject to the constraints of Eq. (3) with two corresponding Lagrangian multiplier functions, $v_s^\alpha(\mathbf{r})$ and $v_s^\beta(\mathbf{r})$,

$$W^\sigma[v_s^\sigma] = \sum_i^{N^\sigma} \langle \phi_i^\sigma | \hat{T} | \phi_i^\sigma \rangle + \int v_s^\sigma(\mathbf{r}) (\rho^\sigma(\mathbf{r}) - \rho_0^\sigma(\mathbf{r})) d^3r \quad \text{for } \sigma = \alpha, \beta. \quad (7)$$

Following Ref. 39, the local potentials which yield the target α - and β -electron densities can now be determined by the unconstrained maximization of $W^\sigma[\rho^\sigma(\mathbf{r})]$ with respect to the local potential $v_s^\sigma(\mathbf{r})$ for each electron spin σ .

To perform this maximization, the local potential is expanded in a finite basis set as [38,39],

$$v_s^\sigma(\mathbf{r}) = v_{\text{ext}}(\mathbf{r}) + v_{\text{Coul}}[\rho_0](\mathbf{r}) + v_0(\mathbf{r}) + \sum_t b_t^\sigma g_t(\mathbf{r}), \quad (8)$$

where $v_{\text{nuc}}(\mathbf{r})$ is the nuclear potential, $v_{\text{Coul}}(\mathbf{r})$ is the Coulomb potential of the target density $\rho_0 = \rho_0^\alpha + \rho_0^\beta$, and $v_0(\mathbf{r})$ represents an initial guess for the exchange–correlation potential, while the remainder is expressed as a linear combination of a finite set of basis functions $\{g_t(\mathbf{r})\}$ with coefficients $\{b_t^\sigma\}$. For fixed $v_{\text{ext}}(\mathbf{r})$ and $v_0(\mathbf{r})$, the unconstrained maximization of $W^\sigma[v^\sigma]$ turns into an extremum problem with respect to the expansion coefficients $\{b_t^\sigma\}$ for each electron spin. The first and second derivatives of $W^\sigma[\rho^\sigma(\mathbf{r})]$ with respect to $\{b_t^\sigma\}$ can be calculated analytically and one obtains [39] the following expression for the gradient,

$$\frac{\partial W^\sigma}{\partial b_t^\sigma} = \int g_t(\mathbf{r}) (\rho^\sigma(\mathbf{r}) - \rho_0^\sigma(\mathbf{r})) d^3r \quad (9)$$

and the Hessian,

$$H_{st} = \frac{\partial^2 W^\sigma}{\partial b_s^\sigma \partial b_t^\sigma} = 2 \sum_i^{\text{occ}^\sigma} \sum_a^{\text{unocc}^\sigma} \frac{\langle \phi_i^\sigma | g_s | \phi_a^\sigma \rangle \langle \phi_a^\sigma | g_t | \phi_i^\sigma \rangle}{\varepsilon_i^\sigma - \varepsilon_a^\sigma}, \quad (10)$$

for each electron spin σ . Note that Eqs. (9) and (10) are simplified for the case of real-valued orbitals here. With the gradient and Hessian available, the maximization can be performed using a standard Newton–Raphson optimization.

If a finite basis sets is employed for representing the KS orbitals, the potential reconstruction turns into an ill-posed problem and the optimized potentials resulting from the Wu-Yang direct optimization as described here are not unique [40, 41, 58]. This can be seen [46] by considering a change in the local α - or β -electron potential $\Delta v_s^\sigma(\mathbf{r}) = v_s^\sigma(\mathbf{r}) - v_{s,0}^\sigma(\mathbf{r})$, where $v_{s,0}^\sigma(\mathbf{r})$ is the potential obtained from the direct optimization, generating the orbitals $\{\phi_i^\sigma\}$ and $\{\phi_a^\sigma\}$. To first order, this change $\Delta v_s^\sigma(\mathbf{r})$ induces a response in the density,

$$\Delta\rho^\sigma(\mathbf{r}) = 2 \sum_i^{\text{occ}^\sigma} \sum_a^{\text{unocc}^\sigma} \frac{\langle \phi_a^\sigma | \Delta v_s^\sigma | \phi_i^\sigma \rangle}{\epsilon_i^\sigma - \epsilon_a^\sigma} \phi_i^\sigma(\mathbf{r}) \phi_a^\sigma(\mathbf{r}), \quad (11)$$

with $\Delta v^\sigma(\mathbf{r}) = \sum_t \Delta b_t^\sigma g_t(\mathbf{r})$ and $\Delta b_t^\sigma = b_t^\sigma - b_{t,0}^\sigma$. Here, one notices that any change in the potential $\Delta v_s^\sigma(\mathbf{r})$ will leave the electron density unchanged if $\langle \phi_a^\sigma | \Delta v_s^\sigma(\mathbf{r}) | \phi_i^\sigma \rangle = 0$. Hence, if the orbital basis is not flexible enough, the α - and β -electron densities are not affected by certain changes, e.g., oscillations, in the respective potentials. Linear combinations of basis functions $g_t(\mathbf{r})$ for which the condition $\langle \phi_a^\sigma | \Delta v_s^\sigma(\mathbf{r}) | \phi_i^\sigma \rangle = 0$ holds are obtained by inserting the basis set expansion for the potential and performing a singular value decomposition (SVD) of the matrix $B_{ai,t}^\sigma = \langle \phi_a^\sigma \phi_i^\sigma | g_t \rangle / (\epsilon_i^\sigma - \epsilon_a^\sigma)$, which leads to

$$\Delta\rho^\sigma(\mathbf{r}) = 2 \sum_r s_r^\sigma \Delta \tilde{b}_r^\sigma \tilde{\Phi}_r^\sigma(\mathbf{r}), \quad (12)$$

where $\{s_r^\sigma\}$ are the singular values of \mathbf{B}^σ and where $\Delta \tilde{b}_r^\sigma = \sum_t V_{t,r}^\sigma \Delta b_t^\sigma$ and $\tilde{\Phi}_r^\sigma(\mathbf{r}) = \sum_{ia} U_{ia,r}^\sigma \phi_i^\sigma(\mathbf{r}) \phi_a^\sigma(\mathbf{r})$ are the expansion coefficients of the change in the potential and the occupied–virtual orbital products transformed with the left and right singular vectors, $(V_{t,r}^\sigma)$ and $(U_{ia,r}^\sigma)$, respectively. Here, the transformed expansion coefficients \tilde{b}_r^σ refer to the transformed potential basis functions $\tilde{g}_r^\sigma(\mathbf{r}) = \sum_t V_{t,r}^\sigma g_t(\mathbf{r})$. Thus, we notice that if one of these transformed potential basis functions $\tilde{g}_r^\sigma(\mathbf{r})$ corresponds to a singular value s_r that is zero or very small, the corresponding expansion coefficient $\tilde{b}_r^\sigma(\mathbf{r})$ can be changed (almost) freely without affecting the density. Therefore, an additional criterion is necessary for singling out the optimal optimized potential among those yielding the same density within the finite basis set.

2.3 Choosing the Optimal Optimized Potential

One possibility for unambiguously singling out an optimized potential was suggested in Ref. [46]. This scheme starts from the requirement that the optimized potential obtained with a finite orbital basis set should be as close as possible to the one obtained in the basis set limit. Specifically, the density calculated from the optimal optimized potential should still agree with the target density $\rho_0^\alpha(\mathbf{r})$ or $\rho_0^\beta(\mathbf{r})$. Thus, we introduce a complete set of virtual orbitals (see Ref. [46] for details),

$$\tilde{\phi}_{\mathbf{r}}^\sigma(\mathbf{r}') = \delta(\mathbf{r} - \mathbf{r}') - \sum_j^{\text{occ}\sigma} \phi_j^\sigma(\mathbf{r}') \phi_j^\sigma(\mathbf{r}), \quad (13)$$

with the Dirac delta function $\delta(\mathbf{r} - \mathbf{r}')$ and where the second term ensures the orthogonality of $\tilde{\phi}_{\mathbf{r}}^\sigma(\mathbf{r}')$ and the occupied orbitals $\phi_i^\sigma(\mathbf{r})$. With this complete representation of the virtual orbital space, the change in the electron density due to a variation in the potential [Eq. (11)] can be approximated as

$$\Delta\rho^\sigma(\mathbf{r}) \approx \sum_i^{\text{occ}\sigma} \phi_i^\sigma(\mathbf{r}) \langle \tilde{\phi}_{\mathbf{r}}^\sigma | \hat{T} + v_s^\sigma | \phi_i^\sigma \rangle. \quad (14)$$

For singling out the optimal potential, we search for the potential for which the electron density does not change considerably when the orbital basis is enlarged, and minimize

$$\int \frac{\Delta\rho(\mathbf{r})^2}{\rho(\mathbf{r})} d^3r \approx \int \frac{1}{\rho^\sigma(\mathbf{r})} \left[\sum_i^{\text{occ}\sigma} \phi_i^\sigma(\mathbf{r}) \langle \tilde{\phi}_{\mathbf{r}}^\sigma | \hat{T} + v_s^\sigma | \phi_i^\sigma \rangle \right]^2 d^3r \rightarrow \min. \quad (15)$$

Here, the inverse density has been introduced as a weighting function (i.e., the relative change in the density is minimized) to obtain a uniformly accurate potential. As is discussed in Ref. [46], this choice can also be justified using theoretical arguments. The minimization then leads to the linear systems of equations $\mathbf{A}^\sigma \Delta \mathbf{b}^\sigma = -\mathbf{z}^\sigma$ with [46],

$$A_{st}^\sigma = \sum_{ij}^{\text{occ}\sigma} \int \frac{\phi_i^\sigma(\mathbf{r}) \phi_j^\sigma(\mathbf{r})}{\rho^\sigma(\mathbf{r})} \langle \tilde{\phi}_{\mathbf{r}}^\sigma | \tilde{g}_s^\sigma | \phi_i^\sigma \rangle \langle \tilde{\phi}_{\mathbf{r}}^\sigma | \tilde{g}_t^\sigma | \phi_j^\sigma \rangle d^3r \quad (16)$$

and

$$z_t^\sigma = \sum_{ij}^{\text{occ}\sigma} \int \frac{\phi_i^\sigma(\mathbf{r}) \phi_j^\sigma(\mathbf{r})}{\rho^\sigma(\mathbf{r})} \langle \tilde{\phi}_{\mathbf{r}}^\sigma | \hat{h}_0^\sigma | \phi_i^\sigma \rangle \langle \tilde{\phi}_{\mathbf{r}}^\sigma | \tilde{g}_t^\sigma | \phi_j^\sigma \rangle d^3r \quad (17)$$

where $\hat{h}_0^\sigma = -\Delta/2 + v_s^\sigma(\mathbf{r})$. This problem can be solved directly, without explicitly solving the KS equations using an extended orbital basis set. Results obtained using this scheme will be referred to as “*optimal (full)*” in the following.

For comparison, we will also employ two additional schemes for singling out one optimized potential. The first one, called “*balanced*” in the following, is based on the idea that a unique potential is also obtained if the potential basis set is chosen such that it is balanced with respect to the orbital basis set [42]. This can be achieved by only retaining those transformed potential basis functions $\tilde{g}_r^\sigma(\mathbf{r})$ corresponding to singular values s_r that are not too small, i.e., above a chosen threshold s_{thr} . This is closely related to the OEP scheme of Kollmar and Filatov [43]. Note that in the spin-unrestricted case considered here, such a scheme effectively employs different potential basis sets for the α - and β -spin potentials.

In addition, we also use a criterion for singling out the optimized potentials that are as smooth as possible (labelled “*smooth*” in the following). To this end, we minimize the norm of the gradient of the potential,

$$\int |\nabla v_s^\sigma(\mathbf{r})|^2 d^3r = \int \left[\sum_t b_t^\sigma \nabla g_t^\sigma(\mathbf{r}) \right]^2 d^3r \rightarrow \min, \quad (18)$$

under the constraint that the change in the density [Eq. (12)] is below a chosen threshold e_{thr} . This results in a quadratic programming problem that can be solved using standard approaches [46]. This criterion is in close analogy to the method of Yang and coworkers [41, 45, 62], who introduced a similar constraint by employing a penalty function during the direct optimization. Note that a common feature of all three approaches presented here is that they are applied *a posteriori*, and hence a direct optimization of the potentials must be performed first. This first step then provides a non-unique potential and corresponding orbitals, which are required for the following second step.

3 Computational Methodology

All finite basis set calculations were performed with a local version of the Amsterdam Density Functional (ADF) program package [63] together with the PYADF scripting framework [64]. To allow for the treatment of spin-unrestricted target densities, we extended our recent implementation [30] of the Wu–Yang direct optimization algorithm and of the subsequent step for singling out an unambiguous optimized potential [46].

The TZ2P and QZ4P Slater-type orbital (STO) basis sets of ADF were used as orbital basis. The potential was expanded in a finite basis set [Eq. (8)], using ADF’s density fitting basis sets corresponding to the TZ2P or QZ4P orbital basis sets. In all calculations, these basis sets were augmented with additional $1s$ functions in an even-tempered fashion (see Supporting Information for details). As initial guess for the potential, we used a scaled version of the Fermi–Amaldi potential [46, 53] of the fixed target electron density $\rho_0(\mathbf{r}) = \rho_0^\alpha(\mathbf{r}) + \rho_0^\beta(\mathbf{r})$, namely

$$v_0(\mathbf{r}) = v_{\text{FA}}[\rho_0](\mathbf{r}) = -\frac{\xi}{N} \int \frac{\rho_0(\mathbf{r}')}{|\mathbf{r} - \mathbf{r}'|} d^3r', \quad (19)$$

where ξ represents the most diffuse exponent in the STO orbital basis set. This scaled Fermi–Amaldi potential ensures that the optimized local potentials have the correct long-range behavior. In the case of target densities obtained from wave-function based *ab initio* calculations, which employed Gaussian-type orbital (GTO) basis sets, the Coulomb potential $v_{\text{Coul}}[\tilde{\rho}_0]$ and Fermi–Amaldi potential $v_{\text{FA}}[\tilde{\rho}_0]$ in Eq. (8) are evaluated for an approximate reference density $\tilde{\rho}_0(\mathbf{r})$ obtained from a DFT calculation in ADF in which the orbitals are expanded in STO basis functions.

If large basis sets are employed for the potential, the Hessian matrix of Eq. (10) contains many small eigenvalues which decay gradually to zero. This causes convergence problems during the Newton–Raphson optimization, which we previously addressed by ignoring eigenvalues below a certain threshold. However, for *ab initio* target densities expanded in GTOs, this scheme still caused poor convergence behavior. Therefore, we followed the work of Wu and

Yang [65] and performed a singular value decomposition (SVD) of the Hessian \mathbf{H} . Then the inverse Hessian can be expressed as

$$\mathbf{H}^{-1} = \mathbf{U} \text{diag}(1/\sigma_r) \mathbf{V}^T, \quad (20)$$

where the columns of \mathbf{U} and \mathbf{V} are the left and right singular vectors, respectively, for the corresponding singular values s_r . To this inverse Hessian, a Tikhonov regularization [66, 67] is applied by replacing it by

$$\mathbf{H}^{-1} = \mathbf{U} \text{diag}(f_r/\sigma_r) \mathbf{V}^T, \quad (21)$$

where f_r is a filter factor, which is chosen as

$$f_r = \frac{\sigma_r^2}{\sigma_r^2 + \lambda^2}. \quad (22)$$

We found that appropriate values for the parameter λ turn out to be $10^{-4} \leq \lambda \leq 0.01$. If $\sigma_r \gg \lambda$, the filter factor f_r is approximately one, while in the case of $\sigma_r \ll \lambda$, f_r approaches zero. Thus, instead of abruptly discarding small singular values, the Tikhonov regularization cuts them off gradually.

As convergence criterion for the Wu–Yang direct optimization, we used the absolute error in the α - and β -electron densities Δ_{abs} compared to the target α - and β -electron densities, defined as

$$\Delta_{\text{abs}}^{\sigma} = \int |\rho^{\sigma}(\mathbf{r}) - \rho_0^{\sigma}(\mathbf{r})| d^3r. \quad (23)$$

The minimal absolute error that can be achieved depends on the considered system, as will be discussed below.

When singling out the optimal potential according to the scheme of Ref. [46], regions in which the electron density is very small turn out to be problematic. This is because for densities expanded in finite GTO or STO basis sets, the exact potential in these regions shows artifacts caused by unphysical nodes in the density [68, 69]. To avoid these artifacts, grid points at which the reconstructed α - or β -electron densities are smaller than a threshold

are ignored when constructing the right-hand side \mathbf{z}^σ according to Eq. (17). This corresponds to assuming that the optimized potentials are already well approximated by the initial guess if the difference between the target and reconstructed density is smaller than the threshold. For the lithium atom, this threshold was chosen as 10^{-4} , whereas for the dioxygen molecule it was set to 10^{-8} .

For target densities expanded in STOs, the exchange–correlation potential is obtained by adding the Fermi–Amaldi potential to the part of the potential expanded in basis functions [cf. Eq. (8)]. In the case of target densities obtained in GTOs, the final exchange–correlation potentials for α - and β -electrons are obtained as

$$v_{\text{xc}}^\sigma(\mathbf{r}) = (v_{\text{Coul}}[\tilde{\rho}_0](\mathbf{r}) - v_{\text{Coul}}[\rho_{\text{WY}}](\mathbf{r})) + v_{\text{FA}}[\tilde{\rho}_0](\mathbf{r}) + \sum_t b_t^\sigma g_t(\mathbf{r}). \quad (24)$$

Here, the first term accounts for the difference between the Coulomb potential used as initial guess (evaluated for the density $\tilde{\rho}_0$) and the Coulomb potential corresponding to the target density ρ_0 . The latter is approximated by the density ρ_{WY} obtained in a STO expansion from the Wu–Yang optimization before singling out an unambiguous potential, as this density represents to the best available STO representation of the GTO target density.

To obtain numerical reference potential for atoms, we employed a modified van Leeuwen–Baerends algorithm [16] in combination with a numerical solution of the KS equations on a logarithmic radial grid [70, 71], as described in Ref. [46]. Here, we used the same initial guess for the potential, and updated the potential iteratively until the absolute error $\Delta_{\text{abs}}^\sigma$ compared to the target α - and β -electron densities was each below $10^{-4} \text{ e bohr}^{-3}$.

All CASSCF calculations for obtaining accurate *ab initio* target densities were performed with the MOLPRO program package [72] using Dunning’s cc-pVTZ basis set for all atoms [73, 74]. For the lithium atom, all electrons are correlated in all orbitals [corresponding to a full configuration interaction (Full-CI) treatment], while for the oxygen molecule the electron (spin) density from a CAS(12,12)SCF calculation was employed. Here, we verified that the resulting densities are converged with respect to the dimension of the active space.

4 Optimized Potentials from Spin Densities

4.1 The Lithium Atom

BP86 target (spin) density expanded in STOs

As a simple test case, we consider the lithium atom. In its doublet ground-state, there are two α -electrons and one β -electron, i.e., one unpaired electron. First, we use the α - and β -electron densities from a unrestricted KS-DFT calculation employing the QZ4P orbital basis set and the BP86 exchange–correlation functional as target. Here, it should be possible to reconstruct the target (spin) density accurately in a potential reconstruction using the same orbital basis set. The target total and spin densities are shown in Fig. 1. For the lithium atom, there is only minimal spin polarization and the spin density is determined by the unpaired electron in the $2s$ orbital, whereas almost identical $1s$ orbitals are obtained for α - and β -electrons (see also Fig. 1 in the Supporting Information).

[Figure 1 about here.]

For assessing the quality of the optimized potentials obtained with finite orbital basis sets, we determined the exchange–correlation potentials for α - and β -electrons numerically as described above. These are presented in Fig. 2 as reference (black line) alongside the potentials obtained from potential reconstruction calculations employing the finite QZ4P orbital basis set and the corresponding QZ4P density fitting basis set augmented with additional tight $1s$ functions for expanding the potential. In addition, we included the BP86 exchange–correlation potential evaluated for the target density (blue dashed line), i.e., the potential that was used in the finite-basis set KS-DFT calculation for determining the target α - and β -electron densities. We note that, even though it is close to it, this BP86 potential does not agree with the numerical reference potential. As was pointed out before, these two potentials should only be equal in the basis set limit [46, 69].

[Figure 2 about here.]

The reconstructed α - and β -electron exchange–correlation potentials $v_{xc}^\alpha(\mathbf{r})$ and $v_{xc}^\beta(\mathbf{r})$ are shown in Figs. 2a and 2b. In both cases, the potentials obtained from the Wu–Yang optimization in the first step show large oscillations and are, therefore, not shown in the figures. These oscillations are removed if an unambiguous potential is singled out in the second step. Irrespective of which of the schemes described in Section 2.3 is applied, the potentials closely agree with the numerical reference for $r > 0.5$ bohr. However, differences are found closer to the nucleus (see also the insets in Fig. 2). When using an implicitly balanced potential basis set (dashed red line), the potential is too large close to the nucleus. The α -electron potential has a spurious minimum in this case and show slight oscillations around the numerical reference potential. Singling out the potential that is as smooth as possible (solid magenta line) does not introduce oscillations, but also results in a potential with the wrong behavior for small r . On the other hand, the optimal potential determined using the criterion of Eq. (15) closely matches the numerical reference potential also close to the nucleus.

[Table 1 about here.]

For a more quantitative comparison of the different approaches, we present the absolute errors $\Delta_{\text{abs}}^{\sigma, \text{num}}$ [cf. Eq.(23)] in the α - and β -electron densities obtained from the different potentials in a numerical solution of the KS equations compared to the target α - and β -electron densities in Table I. Naturally, this absolute error is the smallest for the numerical reference potential. For the α -electron potentials, the largest error is obtained for the potential obtained from the Wu–Yang optimization with ca. 10^{-2} e bohr $^{-3}$, i.e., the error is two magnitudes larger than for the numerical reference. This error is only slightly reduced by using an implicitly balanced basis set or by singling out a smooth potential. In contrast, for the optimal potential, the absolute error in the numerical density is reduced by an order of magnitude below 10^{-3} e bohr $^{-3}$. A similar picture is obtained for the β -electron potentials, even though all

the errors are smaller in this case. Thus, these results confirm the previous finding that high-quality potentials can be obtained by applying the criterion of Eq. (15) for unambiguously singling out the optimal potential [46].

In addition to the errors in the densities obtained from a numerical solution of the KS equations with the different potentials, Table I also includes the absolute errors $\Delta_{\text{abs}}^{\sigma, \text{finite}}$ obtained with these potentials in the finite orbitals basis set. In this case, the smallest error is obtained for the potentials obtained directly from the Wu-Yang optimization, and these absolute errors correspond to the convergence criterion used in this step. After singling out one optimized potential in the second step the error increases, but the smallest one is obtained for the optimal potential. Note that for both the optimal and the numerical reference potential the absolute density errors are larger in the finite orbital basis set than for the numerical solution of the KS equations. This discrepancy was discussed previously [46] and arises because it is in general not possible to reproduce the target density both in a given finite basis set and in a fully numerical calculation at the same time. However, as was noted before, these differences decrease when increasing the size of the orbital basis set.

After assessing the quality of the reconstructed α - and β -electron exchange–correlation potentials, we turn to Figs. 2c and Figs. 2d, where the same results are shown as total exchange–correlation potentials $v_{\text{xc}}^{\text{tot}}(\mathbf{r}) = \frac{1}{2}(v_{\text{xc}}^{\alpha}(\mathbf{r}) + v_{\text{xc}}^{\beta}(\mathbf{r}))$ and spin exchange–correlation potentials $v_{\text{xc}}^{\text{spin}}(\mathbf{r}) = \frac{1}{2}(v_{\text{xc}}^{\alpha}(\mathbf{r}) - v_{\text{xc}}^{\beta}(\mathbf{r}))$, respectively. While for the total potential, the overall results are similar to those discussed for the individual spin components, it is apparent that reconstructing the spin potential accurately is significantly more difficult. To calculate the difference between the α -electron potential and the β -electron potential reliably, it is necessary to determine each of these individual α - and β -electron potentials with comparable accuracy.

For the lithium atom considered here, the spin polarization is very small. Therefore, the spin part of the exchange–correlation potential is very small as well. In particular, it is almost

constant in the range probed by the $1s$ orbital and, therefore, does not introduce a significant spin polarization for the $1s$ orbital. Thus, the spin potential is mostly due to the different asymptotic decay of the α - and β -electron densities. Since the BP86 exchange–correlation potentials evaluated from the target α - and β -electron densities do not show the correct asymptotic decay, the corresponding spin potential almost vanishes. Even though the spin potential is evaluated as the difference of the much larger α - and β -electron potentials, the optimal potential reproduces the numerical reference almost perfectly. On the other hand, the smooth and the balanced potential deviate from the numerical reference not only close to the nuclei (where these differences were also recognizable for the α - and β -spin potentials), but also further away from the nuclei. Thus, in order to reconstruct the spin potential $v_{xc}^{\text{spin}}(\mathbf{r})$ reliably, it is essential to single out the optimal potential according to the criterion of Eq. (15).

Full-CI target (spin) density expanded in GTOs

Next, we use the accurate α - and β -electron densities from a Full-CI calculation for the lithium atom as our target. In this case, the target α - and β -electron densities have to be expanded in a GTO orbital basis set, which might result in additional difficulties when performing the potential reconstruction with our implementation using an STO orbital basis set. The Full-CI total and spin densities are included in Fig. 1 and are on the scale of the plots almost indistinguishable from the BP86 ones considered above. Nevertheless, the difference densities also included in Fig. 1 show that there are slight differences, in particular for the $1s$ orbital density and the asymptotic decay.

[Figure 3 about here.]

Fig. 3 shows the reconstructed total and spin exchange–correlation potentials, whereas the individual α - and β -electron potentials are presented in Fig. 2 in the Supporting Information.

The potentials obtained from the Full-CI density with a numerical solution of the KS equations are included as black dashed lines in these plots. These reference potentials features considerable oscillations which are most pronounced near the nucleus. Such an oscillatory behavior in the reconstructed potentials is commonly found when the target density is expanded in a set of Gaussian-type orbitals (GTOs) [75] and can be attributed to the deficiency of GTOs to represent the correct form of the electron density close to the nucleus. However, these oscillations can be reduced when the GTO orbital basis set used for determining the target density is enlarged [75]. This is shown in Fig. 3 in the Supporting Information by comparing numerical potentials reconstructed from the Full-CI/cc-pVTZ target density and from a CAS(3,30)SCF/cc-pVQZ target density.

As a first step of the potential reconstruction, we determine a (non-unique) potential using the Wu–Yang direct optimization algorithm. Here, we apply two different STO orbital basis sets (TZ2P and QZ4P) in combination with the corresponding density fitting basis sets augmented with additional tight $1s$ functions for expanding the potential. While for the BP86 target density expanded in STOs this optimization could be converged until the absolute error in the density was smaller than $8.0 \cdot 10^{-4}$ and 10^{-4} e bohr $^{-3}$ for the α - and β -electron density, respectively, looser convergence criteria have to be used for the GTO target densities. With a TZ2P orbital basis set, the absolute density error in the Wu–Yang optimization only reaches $5.1 \cdot 10^{-3}$ and $2.0 \cdot 10^{-3}$ e bohr $^{-3}$ for the α - and β -electron density, respectively (see Tab. II). This is further reduced to $2.5 \cdot 10^{-3}$ and $4.0 \cdot 10^{-4}$ e bohr $^{-3}$, respectively, with the larger QZ4P orbital basis set. The corresponding difference densities are shown in the upper insets in Fig. 1. Thus, a sufficiently large STO orbital basis set is required to be able to represent the target density from an *ab initio* calculation using GTOs. Nevertheless, with the QZ4P basis set it is possible to achieve an agreement close to the one obtained for the target density expanded in STOs. We note that the methodological improvements discussed in Section 3, in particular the use of the Tikhonov regularization, are essential here to make this convergence possible.

[Table 2 about here.]

Since the numerical potential reconstructed from the GTO densities show oscillations due to the insufficiencies of the GTO basis set close to the nucleus, we also performed a numerical potential reconstruction using the α - and β -electron densities from the Wu–Yang optimization, which are expanded in an STO orbital basis, as target. These are included in Fig. 3 as solid black line. They do not show oscillations near the nucleus anymore, but otherwise closely match the numerical potentials reconstructed from the GTO densities. However, for the TZ2P orbital basis set, the total and spin potentials reconstructed from the STO and GTO densities differ significantly for $r > 2$ bohr. This can be traced back to the β -electron potential (see Fig. 2 in the Supporting Information), and is caused by spurious nodes appearing in the β -electron density in the region where it is very small [68, 69]. The β -electron density in the lithium atom is particularly prone to such artifacts because it is due to only one orbital, i.e., nodes in this orbital are not offset by other (nonzero) orbitals. In the following, we will consider the numerical potentials reconstructed from the Wu–Yang densities expanded in STOs as reference for the finite-basis set potential reconstruction.

The optimized potentials obtained from the finite-basis set reconstruction using the different schemes for singling out one unambiguous potential after the Wu–Yang optimization are included in Fig. 3. The potentials obtained directly from the Wu–Yang optimization contain considerable oscillations and are hence not shown in the figure. First, we consider the total exchange–correlation potentials in Figs. 3a and 3c (for the individual α - and β -electron potentials, see Fig. 2 in the Supporting Information). With the TZ2P orbital basis set, both the smooth and the optimal potential show a good agreement with the numerical reference potential for $r < 2$ bohr, whereas the potential obtained with an implicitly balanced potential basis set still features some small oscillations. For $r < 2$ bohr, none of the potentials can reproduce the bump in the reference potential caused by artifacts of the β -electron density in this region. In principle, the optimal potential should account for this feature, since the criterion of Eq. (15) minimizes the deviation from the Wu–Yang density in the

basis-set limit, i.e., it should converge to the numerical reference potential determined from that density. However, as discussed in Section 3, regions where the density is smaller than 10^{-4} e bohr $^{-3}$, which is reached for the β -electron density at $r > 2$ bohr, are discarded in our implementation to avoid such artifacts at small densities. In fact, we verified that after increasing the threshold for discarding small densities, the optimal potential does account for the bump in the reference potential.

When increasing the size of the orbital basis set to QZ4P, the total exchange–correlation potentials from all three schemes closely agree with the numerical reference. Differences only remain for the smooth and balanced potentials close to the nucleus, while the optimal potential matches the reference also in this region. For a more quantitative comparison, the absolute errors $\Delta_{\text{abs}}^{\sigma, \text{num}}$ in the α - and β -electron densities obtained from the different potentials in a numerical solution of the KS equations compared to the target α - and β -electron densities are listed in Table II. In all cases, the smallest error is achieved for the optimal potential. Moreover, the absolute errors in the numerical densities decrease for all three schemes when going from the TZ2P to the QZ4P orbital basis set.

In addition, Table II includes the absolute errors $\Delta_{\text{abs}}^{\sigma, \text{finite}}$ in the α - and β -electron densities obtained with the different potential in the finite orbital basis set. In general, these errors increase compared to the potentials obtained from the Wu–Yang procedure when applying the schemes for singling out one optimized potential. For the TZ2P orbital basis, the largest error in the α -electron density within the finite basis set is in fact obtained for the optimal potential, even though for this potential the error in the numerical density is the smallest. Again, this is because the error in the finite-basis set density and in the numerical density cannot be minimized at the same time [46]. Note that the finite-basis set density error with the optimal potential is comparable to the one obtained with the numerical reference potential. When going to the larger QZ4P orbital basis set, the finite-basis set density errors decrease significantly, both for the optimal and for the numerical reference potentials. This can also be seen in the finite-basis set difference densities obtained with the optimal

potentials, which are included in the lower insets in Fig. 3.

Finally, we turn to the reconstructed spin exchange–correlation potentials shown in Fig. 3b and 3d. Again, reproducing the numerical reference potential is much more difficult in this case because the spin potential is calculated as the difference of the α - and β -electron potentials. Therefore, even though with the TZ2P orbital basis set, the smooth potential visually agrees with the reference for the total and the individual α - and β -electron potentials at $r < 2$ bohr (see Fig. 3a and Figs. 2a and 2b in the Supporting Information), the corresponding spin potential deviates significantly. On the other hand, the optimal potential shows a good agreement with the numerical reference for $r < 2$ bohr and only fails to reproduce the spurious behavior for larger r (see discussion above). With the QZ4P orbital basis set, the agreement with the numerical reference improves for all reconstructed potentials. However, for the potential obtained with an implicitly balanced basis set, there are still significant oscillations, which are not obvious in the plots of the individual α - and β -electron potentials (see Figs. 2c and 2d in the Supporting Information). The smooth potential qualitatively reproduces all features of the numerical reference, but the best agreement is achieved for the optimal potential.

The comparison of the TZ2P and the QZ4P orbital basis sets demonstrates that the optimal potentials obtained with the smaller TZ2P orbital basis already agree very well with the numerical reference potential determined from the Wu–Yang density, which corresponds to the closest available approximation of the target density in the STO orbital basis. However, this Wu–Yang density differs from the target density expanded in GTOs so that deviations to the numerical potential determined from that target density occur. Thus, the QZ4P orbital basis set is required in order to obtain a (spin) potential that agrees with the numerical potential calculated from the GTO target density not because of the basis set requirements of the scheme for singling out the optimal potential, but because of the need to reproduce the target density represented in an GTO basis set with STOs in the Wu–Yang optimization step. However, the use of an STO representation of the density in the first step before

determining the optimal potential according to the criterion of Eq. (15) has the advantage of avoiding the spurious oscillations in the reconstructed potential arising for a GTO expansion of the target density close to the nucleus. Of course, a sufficiently large STO basis set will be able to reproduce the spurious behavior of the GTO density close to the nucleus and will result in a potential showing the corresponding oscillatory behavior.

Finally, we note that the optimal potentials presented here are converged with respect to the size of the potential basis set. Adding additional tight or diffuse functions does not alter the resulting optimal potentials significantly anymore. The dependence of the optimal potentials on the potential basis set is illustrated in Figs. 4 and 5 and Table I and II in the Supporting Information.

4.2 An Open-Shell Molecule: Dioxygen

BP86 target (spin) density expanded in STOs

We now investigate a diatomic molecule with an open-shell ground state, namely dioxygen O_2 with an O–O bond distance of 1.21 Å in its equilibrium structure. Here, the two antibonding π^* -orbitals are singly occupied. First, we consider a target density from an unrestricted KS-DFT calculation using the BP86 exchange–correlation functional and the Slater-type QZ4P orbital basis set. This target spin density is shown in Fig. 4a and 4b along the bonding axis (x -axis) and perpendicular to it (y -axis), respectively. Along the y -axis, the spin density is determined by the singly occupied orbitals which have a cylindrical shape around the bond axis, as is also visible in the plot of the spin density in the xy -plane in Fig. 4c. On the other hand, the singly occupied orbitals vanish on the bond axis and, therefore, the spin density along the x -axis is solely due to the spin polarization of the doubly occupied orbitals (i.e., the differences between the occupied α - and β -electron orbitals). In particular, there is a region where the spin density becomes negative (see the yellow regions in Fig. 4c).

[Figure 4 about here.]

The total exchange–correlation potentials reconstructed for the dioxygen molecule from the BP86/QZ4P target density using the different scheme for singling out an unambiguous potential are shown in Fig. 5a and b along the bond axis and perpendicular to it, respectively. For comparison, the figures include the BP86 exchange–correlation potential calculated from the target density, i.e., the exchange–correlation potential used for determining the target density. Note, however, that because the finite QZ4P basis set is employed when calculating the target density, this BP86 potential is not equal to the exact potential corresponding to the target density [33, 46].

[Figure 5 about here.]

The different reconstructed total exchange–correlation potentials all agree rather accurately with the BP86 exchange–correlation potential on the scale of the plots. Recognizable differences are only observed along the bond axis in the region between the oxygen atoms. The BP86 potential shows a plateau in this bond region, which is also reproduced when singling out the optimized potential that is as smooth as possible. On the other hand, the balanced as well as the optimal potential do not exhibit such a plateau, but have a maximum at the midbond point. Similar observations can be made for the individual α - and β -electron potentials (see Fig. 7 in the Supporting Information).

[Table 3 about here.]

The absolute errors $\Delta_{\text{abs}}^{\sigma, \text{finite}}$ in the α - and β -electron densities obtained from the different reconstructed potentials within the finite orbital basis set compared to the target densities are listed in Table III. Since the QZ4P orbital basis set used for representing the target density is also employed in the potential reconstruction, the Wu–Yang optimization can be converged such that the error in the α - and β -electron densities is below $2.0 \cdot 10^{-4}$ e bohr⁻³.

This error increases by one order of magnitude for the potential obtained with an implicitly balanced potential basis set and further increases when determining the optimized potential that is as smooth as possible. Note that these errors depend on the choice of the threshold for discarding small singular values s_{thr} and for the change in the density e_{thr} , respectively. For the optimal potential, the finite-basis set absolute error in the α - and β -electron densities increases further to $2.8 \cdot 10^{-2}$ and $2.3 \cdot 10^{-2}$ e bohr $^{-3}$, respectively. The differences between the reconstructed total and the spin densities and the respective target (spin) density is illustrated in Fig. 14 in the Supporting Information. This comparison shows that except for the region close to the nuclei, all reconstructed potentials reproduce all qualitative features of the target spin density.

However, to judge the quality of the different potentials, it would be necessary to determine the absolute errors in the α - and β -electron densities obtained from these potentials in a numerical solution of the KS equations. Unfortunately, this is not easily possible for the molecular system considered here. Nevertheless, for the lithium atom considered above and the atomic systems investigated in Ref. [46], it was demonstrated that this error is the smallest for the optimal potential. Thus, we expect that also for the dioxygen molecule, the optimal potential should be closest to the exact potential, and that the increased absolute errors in the finite basis set arises because it is not possible to reproduce the target density both in a numerical calculation and in the finite QZ4P orbital basis set. Note that the criterion for singling out the optimal potential [Eq. (15)] minimizes the error in the numerical densities, whereas the other approaches minimize the finite-basis set error.

Finally, we turn to the reconstructed spin exchange–correlation potentials, which are presented in Figs. 5c and d. As for the lithium atom, reconstructing this spin potential is more difficult than reconstructing the total potential, because it is determined as the difference between the α - and β -electron potentials and its accurate determination thus requires that these are both obtained with uniform accuracy. In the plots along the bond axis (see Fig. 5c), both the smooth and the balanced spin potentials deviate significantly from the BP86 spin

potential. In particular the latter shows rather pronounced oscillations. Note that these oscillations were not visible in the plots of the individual α - and β -electron potentials, but they are amplified when considering the spin potential. The optimal spin potential plotted along the bond axis shows a more regular form and no oscillations that would appear unphysical, but it also differs from the BP86 spin potential. Nevertheless, except for the spikes at the nuclei themselves, it has a similar overall shape near the nuclei, i.e., a symmetric well in which the potential is smaller at the nucleus than ca. 0.5 bohr away from it. This shape of the spin potential corresponds to the positive spin density close to the nuclei. However, in the midbond region, the shape of the optimal spin potential qualitatively differs from the BP86 spin potential and the optimal spin potential shows a maximum at the midbond point, whereas the BP86 spin potential has a minimum. Here, the maximum of the optimal spin potential is actually in line with the negative spin density at the midbond point. Despite the observed differences, it appears that of the different reconstructed spin potentials, the optimal potential is closest to the BP86 spin potential. Note again that the BP86 spin potential differs from the exact spin potential, which is not available to us here. Furthermore, it is important to recall that the singly occupied orbitals have a node at the bond axis, i.e., the spin potential here is only responsible for the rather small spin polarization of the doubly occupied orbitals (see Fig. 4a) and, therefore, it should be relatively small itself.

[Figure 6 about here.]

When inspecting the reconstructed spin potentials perpendicular to the bond axis (see Fig. 5d), all reconstructed spin potentials qualitatively agree with the BP86 spin potential. Here, the spin potential is significantly larger than along the bond axis, as it now covers the region to which the singly occupied orbitals extend (cf. Fig. 4b). While the differences are small, the optimal spin potential is closest to the BP86 spin potential and only differs at the nucleus, whereas both the smooth and the balanced spin potentials show some oscillatory behavior. The overall shape of the optimal and the BP86 spin potentials in the xy -plane

is compared in Fig. 6. Except for the differences along the bond axis, in particular in the midbond region, already discussed above, we observe a good overall agreement. With the results obtained for the lithium atom in mind, we attribute these differences to the fact that the BP86 potential does not agree with the exact spin potential, and expect that the optimal spin potential is actually a closer approximation to the exact spin potential.

CASSCF (spin) density expanded in GTOs

After considering the reconstruction of the spin exchange–correlation potential for the dioxygen molecule for a BP86/QZ4P target (spin) density, we now turn to an accurate target (spin) density obtained from a CAS(12,12)SCF/cc-pVTZ calculation. This *ab initio* spin density is compared to the BP86 spin density in Fig. 4. Perpendicular to the bond axis (see Fig. 4b), where the spin density is dominated by the unpaired π^* -electrons, the CASSCF spin density qualitatively agrees with the one obtained with BP86, even though the magnitude at the maximum and the asymptotic form slightly differ. Larger differences are found along the bond axis (see Fig. 4a), where the spin density is solely due to the spin polarization of doubly occupied orbitals. The CASSCF spin density is significantly larger close to the nuclei, whereas the negative spin density at the ends of the molecule is reduced. This is also visible in the plot of the CASSCF spin density in the xy -plane shown in Fig. 4d.

[Figure 7 about here.]

While for the BP86/QZ4P target density the BP86 exchange–correlation (spin) potential calculated from the target density could be used for comparison — even though it is not identical to the exact (spin) potential — we now have no reference potential available. Nevertheless, we can still use the results obtained for the BP86 target density to judge whether the (spin) potentials reconstructed from the CASSCF target (spin) density are physically reasonable. The reconstructed total and spin exchange–correlation potentials obtained using a QZ4P orbital basis set using the different scheme for singling out an unambiguous

optimized potential are presented in Fig. 7. The corresponding individual α - and β -electron potentials are given in Fig. 8 in the Supporting Information.

For the reconstructed total exchange–correlation potential, the optimal potential has a similar shape as the BP86 potential discussed above. Along the bond axis (see Fig. 7a), it has a maximum at the midbond point and exhibits some shell structure at ca. 0.5 bohr from the two nuclei. A similar shape as in the outer region along the bond axis is found perpendicular to the bond axis for the optimal potential (see Fig. 7). Both the smooth and the balanced total potentials have a similar shape, but the shell structure is more pronounced. For the balanced total potential, larger oscillations appear close to the nuclei. Nevertheless, the different reconstructed potentials are qualitatively rather similar. A different picture is obtained if the potential reconstruction is performed with the smaller TZ2P orbital basis set, as is shown in Fig. 11 in the Supporting Information. In this case, both the balanced and the smooth total potentials show large oscillations, even though the same thresholds as for the QZ4P orbital basis set are applied. However, the optimal potential is free of such unphysical oscillations already with the smaller orbital basis set. Moreover, the optimal total potential obtained with the TZ2P orbital basis set is on the scale of the figures in good agreement with the one reconstructed using the larger QZ4P orbital basis set.

The absolute errors in the α - and β -electron densities compared to the target densities obtained from these different reconstructed potentials in the finite TZ2P and QZ4P orbital basis sets are listed in Table III. Because we are now trying to reproduce target α - and β -electron densities expanded in a GTO basis set with STOs, these errors are larger than for the BP86 target densities that was represented in the same orbital basis also used in the potential reconstruction. With the TZ2P orbital basis set, the Wu–Yang optimization can be converged until the absolute error is approximately $4 \cdot 10^{-2} \text{ e bohr}^{-3}$ for both the α - and β -electron density. With the larger QZ4P orbital basis set, a slightly smaller error can be achieved for the α -electron density, whereas the error in the β -electron density almost halved for *both* electron spins. With both orbital basis sets, the errors are larger for the smooth and

balanced potentials, with this increase being controlled by the chosen thresholds. For the larger QZ4P orbital basis set, we observe that the increase is smaller than with the TZ2P orbital basis set.

The largest density errors in the finite orbital basis sets are found for the optimal potentials. For the TZ2P orbital basis set, the errors are approximately twice as large as for the Wu–Yang potentials. However, a significantly smaller increase is observed with the QZ4P orbital basis set. Here, we stress again that for judging the quality of the different potentials, it would be necessary to calculate the errors in the densities obtained with a numerical solution of the Kohn–Sham equations on the respective potentials. For the optimal potentials, these numerical density errors, which differ from the finite basis set density errors, should be minimized. With increasing size of the orbital basis set used in the potential reconstruction, the difference between the finite basis set and the numerical density errors should become smaller. Thus, the decrease of the finite basis set density errors when going from TZ2P to QZ4P supports our assumption that the optimal potentials should be closest to the exact potentials. The total and spin densities calculated from the different reconstructed potentials in the finite orbital basis set are compared to the target (spin) density in Fig. 15 in the Supporting Information. Here, it is obvious that these differences are larger than for the BP86 target (spin) density. In particular, the optimal potential yields a spin density that misses some of the qualitative features of the target density around the nuclei. However, it is also apparent that these deviations are reduced when increasing the orbital basis set from TZ2P to QZ4P.

In order to study the convergence of the reconstructed potentials with respect to the potential basis set, we performed additional calculations where additional diffuse functions were included in the potential basis set expansion. The resulting optimal reconstructed potentials are shown in Figs. 16–19 in the Supporting Information, both for the TZ2P and the QZ4P orbital basis set. These results show that the reconstructed potentials are converged with respect to the size of the potential basis set. Only far away from the molecule, i.e., in regions

where the density is very small, some differences between potentials expanded in different basis sets occur. In addition, we observe that the requirements on the potential basis set are most severe for the spin potential, where with the TZ2P orbital basis set increasing the potential basis set still has some effect.

Finally, we now consider the spin exchange–correlation potential, which is shown in Figs. 7c and d along the O–O bond axis and perpendicular to it, respectively. Perpendicular to the bond axis, the optimal spin potential has a similar shape as the one obtained for the BP86/QZ4P target density with a minimum at ca. 0.5 bohr from the oxygen nuclei, i.e., where the spin density is the largest. In contrast, rather pronounced oscillations are observed for the smooth and balanced spin potentials. For the smooth and the balanced spin potentials, such large oscillations are also present in the plot along the bond axis, whereas the optimal potential is mostly well behaved. Qualitatively, it also resembles the optimal spin potential reconstructed from the BP86/QZ4P target density. Around the nuclei, it has negative wells, which are deeper for the CASSCF than for the BP86/QZ4P target density. This is in line with the larger spin density in this region obtained in the CASSCF calculations. In the bond region between the atoms, the optimal spin potential reconstructed from the CASSCF spin density is flatter than in the case of the BP86/QZ4P target density, which agrees with the smaller spin polarization in this region. Very close to the nuclei the reconstructed spin potential has some large oscillations. Most likely, these can be attributed to the deficiencies of the GTO target density, which can cause such oscillations in the exact potentials [75].

[Figure 8 about here.]

To compare the overall performance of the different potential reconstruction schemes, Fig. 8 compares the optimal and the smooth spin potentials in the xy -plane. A similar comparison for the balanced spin potential is shown in Fig. 9 in the Supporting Information. While pronounced wiggling features around the position of the nuclei are found in the smooth spin potential, it is obvious that these can be eliminated in the whole xy -plane for the

optimal spin potential. Thus, even though there is no exact reference spin potential available for comparison, we find that the optimal spin potential is the only one that seems to be free of artifacts of the potential reconstruction. Moreover, the comparison with the spin potential reconstructed from the BP86/QZ4P target density shows that the optimal potential is physically reasonable. Therefore, we are confident that it is the reconstructed potential that is closest to the exact spin potential.

Further support for this conclusion can be drawn from a comparison with the reconstructed potentials obtained for the same CASSCF target density with the smaller TZ2P orbital basis set, which are shown in Fig. 10 and Fig. 12 and 13 in the Supporting Information. Here, even larger oscillations are found for the smooth and balanced spin potentials, even though the same thresholds are applied. On the other hand, the optimal potentials are qualitatively similar to the QZ4P results. This is particularly obvious for the spin potential perpendicular to the bond axis, which is in good agreement with the one reconstructed with the QZ4P orbital basis set. Also along the bond axis the shapes of the optimal spin potentials are similar for the two orbital basis sets, even though the negative well near the oxygen nuclei is less pronounced. Thus, only for the optimal potential a consistent convergence with increasing size of the orbital basis set is observed.

5 Conclusions

In this work, we have extended the unambiguous reconstruction of the local potential yielding a given target density [46] to open-shell systems treated with an unrestricted KS-DFT formalism. Moreover, we have combined this reconstruction with the use of accurate target (spin) densities obtained from accurate wave-function based *ab initio* calculations, i.e., from Full-CI or CASSCF wave functions. This provides a route to accurate reference data for the spin exchange–correlation potential v_{xc}^{spin} , which determines the spin density distribution $Q(\mathbf{r})$ in unrestricted KS-DFT.

Reconstructing this spin exchange–correlation potential is a particularly challenging task, because it is given by the difference between the reconstructed α - and β -electron potentials. Thus, one has to overcome the numerical inaccuracies caused by the ill-posed nature of the potential reconstruction problem in finite orbital basis sets, as these could otherwise be amplified when calculating the spin potential. As test cases, we chose the lithium atom and the oxygen molecule in its triplet state. For both systems, we considered target (spin) densities from unrestricted KS-DFT calculations as well as from Full-CI (for the lithium atom) and CASSCF (for the dioxygen molecule) calculations. These test cases made it possible to systematically assess the quality of the reconstructed spin exchange–correlation potentials.

For the lithium atom, it is possible to compare the reconstructed potentials to the exact ones, which can be obtained from a fully numerical potential reconstruction. The comparison shows that the optimal spin potentials, determined using the scheme of Ref. [46], can reproduce the fully numerical spin potential, while the spin potentials obtained by singling out the α - and β -electron potentials that are as smooth as possible or with an implicitly balanced potential basis set show significantly larger deviations from the reference spin potential. In general, the quality of these smooth and balanced spin potentials strongly depends on the choice of the corresponding threshold values and can result in highly oscillating potentials if these are chosen too small. On the other hand, if these thresholds are too large, the resulting potentials lack all features present in the exact one. Moreover, different thresholds might be required for reconstructing the α - and β -electron potentials in order to obtain these with similar quality, as is required for the reconstruction of the spin potential.

For target densities obtained with GTO orbital basis sets, which are commonly used in wavefunction based *ab initio* calculations, we reconstruct the potential using an STO orbital basis set. This has the advantage that the density obtained from the Wu–Yang optimization, which is the first step in all potential reconstruction schemes tested here, has the correct shape close to the nuclei and in the asymptotic region. Consequently, oscillations close to the

nucleus found in the fully numerical reference potential because of the wrong form the the GTO target density [75] are largely suppressed in the optimal reconstructed potentials. On the other hand, it requires the use of sufficiently large STO orbital basis sets in order to be able to reproduce the *ab initio* target (spin) density. For the lithium atom, we found that the a QZ4P orbital basis set is sufficient to obtain a good agreement with the target density. Moreover, we note that technical improvements to our implementation, in particular the use of a Tikhonov regularization in the Wu–Yang optimization [65] and the use of a cut-off value for discarding small density regions in the criterion of Eq. (15), were necessary to treat GTO target densities.

For the dioxygen molecule, a direct comparison to a fully numerical reference spin potential is not possible. Nevertheless, for the target density obtained from an unrestricted KS-DFT calculation the exchange–correlation potential used for determining the target potential can provide some guidance, even though it differs from the exact potential because of the use of a finite orbital basis set. This comparison shows that the optimal reconstructed spin potential (i.e., the one obtained using the scheme of Ref. [46]) shows the best overall agreement. Also for the CASSCF target density, this scheme is the only one that provides a physically reasonable spin exchange–correlation potential, while the smooth and the balanced potentials are plagued by unphysical oscillations. The optimal potential shows such oscillations only very close to the nuclei, where they are probably due to deficiencies of the GTO expansion used for the target density, and to a smaller extent far away from the molecule.

In summary, we believe that the potential reconstruction scheme proposed in Ref. [46] and extended here to open-shell systems provides the first reliable approach for reconstructing the spin exchange–correlation potential from accurate *ab initio* (spin) densities. The availability of such accurate reference spin potentials can facilitate the development of improved spin-dependent exchange–correlation density functionals which apart from yielding accurate total electron densities also provide reliable spin densities. Thus, this work represents a prerequisite for the design of approximate exchange–correlation functional with an improved

spin-density dependence.

Acknowledgments

M.R. and K.B. gratefully acknowledge financial support by a grant from the Swiss national science foundation (SNF). K.B. thanks the Fonds der Chemischen Industrie for a Chemiefonds scholarship. C.R.J. acknowledges funding from the DFG-Center for Functional Nanostructures (CFN) at KIT.

References

- [1] R. G. Parr and W. Yang, *Density-Functional Theory of Atoms and Molecules*, Oxford University Press, 1989.
- [2] E. Engel and R. M. Dreizler, *Density Functional Theory: An Advanced Course*, Springer, Berlin, 1st edition, 2011.
- [3] W. Koch and M. Holthausen, *A Chemist's Guide to Density Functional Theory*, Wiley, 2001.
- [4] C. J. Cramer and D. G. Truhlar, *Phys. Chem. Chem. Phys.* **11**, 10757 (2009).
- [5] M. Reiher, *Faraday Discuss.* **135**, 97 (2007).
- [6] M. Reiher, *Chimia* **63**, 140 (2009).
- [7] M. Reiher, O. Salomon, and B. A. Hess, *Theor. Chem. Acc.* **107**, 48 (2001).
- [8] M. Reiher, *Inorg. Chem.* **41**, 6928 (2002).
- [9] J. N. Harvey, *Struct. Bond.* **112**, 151 (2004).

- [10] S. Ye and F. Neese, *Inorg. Chem.* **49**, 772 (2010).
- [11] M. Swart, *Int. J. Quantum Chem.* (2012), in press, DOI: 10.1002/qua.24255.
- [12] A. Ghosh, *J. Biol. Inorg. Chem.* **11**, 712 (2006).
- [13] J. Conradie and A. Ghosh, *J. Phys. Chem. B* **111**, 12621 (2007).
- [14] M. Radon and K. Pierloot, *J. Phys. Chem. A* **112**, 11824 (2008).
- [15] K. Boguslawski, Ch. R. Jacob, and M. Reiher, *J. Chem. Theory Comput.* **7**, 2740 (2011).
- [16] R. van Leeuwen and E. J. Baerends, *Phys. Rev. A* **49**, 2421 (1994).
- [17] O. Gritsenko, P. Schipper, and E. Baerends, *Chem. Phys. Lett.* **302**, 199 (1999).
- [18] T. W. Keal and D. J. Tozer, *J. Chem. Phys.* **119**, 3015 (2003).
- [19] T. W. Keal and D. J. Tozer, *J. Chem. Phys.* **121**, 5654 (2004).
- [20] M. J. G. Peach, A. M. Teale, and D. J. Tozer, *J. Chem. Phys.* **126**, 244104 (2007).
- [21] A. M. Teale, S. Coriani, and T. Helgaker, *J. Chem. Phys.* **132**, 164115 (2010).
- [22] P. D. Elkind and V. N. Staroverov, *J. Chem. Phys.* **136**, 124115 (2012).
- [23] J. Karwowski, *Int. J. Quantum Chem.* **109**, 2456 (2009).
- [24] A. S. P. Gomes and Ch. R. Jacob, *Annu. Rep. Prog. Chem. C* **108**, 222 (2012).
- [25] O. Roncero, M. P. de Lara-Castells, P. Villarreal, F. Flores, J. Ortega, M. Paniagua, and A. Aguado, *J. Chem. Phys.* **129**, 184104 (2008).
- [26] O. Roncero, A. Zanchet, P. Villarreal, and A. Aguado, *J. Chem. Phys.* **131**, 234110 (2009).

- [27] P. Elliott, M. H. Cohen, A. Wasserman, and K. Burke, *J. Chem. Theory Comput.* **5**, 827 (2009).
- [28] P. Elliott, K. Burke, M. Cohen, and A. Wasserman, *Phys. Rev. A* **82**, 024501 (2010).
- [29] C. Huang, M. Pavone, and E. A. Carter, *J. Chem. Phys.* **134**, 154110 (2011).
- [30] S. Fux, Ch. R. Jacob, J. Neugebauer, L. Visscher, and M. Reiher, *J. Chem. Phys.* **132**, 164101 (2010).
- [31] J. D. Goodpaster, N. Ananth, F. R. Manby, and T. F. Miller, III, *J. Chem. Phys.* **133**, 084103 (2010).
- [32] J. D. Goodpaster, T. A. Barnes, and T. F. Miller, III, *J. Chem. Phys.* **134**, 164108 (2011).
- [33] P. de Silva and T. A. Wesolowski, *J. Chem. Phys.* **137**, 094110 (2012).
- [34] S. Liu and P. W. Ayers, *Phys. Rev. A* **70**, 022501 (2004).
- [35] Ch. R. Jacob, S. M. Beyhan, and L. Visscher, *J. Chem. Phys.* **126**, 234116 (2007).
- [36] J. D. Talman and W. F. Shadwick, *Phys. Rev. A* **14**, 36 (1976).
- [37] A. Görling, *Phys. Rev. A* **46**, 3753 (1992).
- [38] W. Yang and Q. Wu, *Phys. Rev. Lett.* **89**, 143002 (2002).
- [39] Q. Wu and W. Yang, *J. Chem. Phys.* **118**, 2498 (2003).
- [40] V. N. Staroverov, G. E. Scuseria, and E. R. Davidson, *J. Chem. Phys.* **124**, 141103 (2006).
- [41] T. Heaton-Burgess, F. Bulat, and W. Yang, *Phys. Rev. Lett.* **98**, 256401 (2007).
- [42] A. Heßelmann, A. W. Götz, F. Della Sala, and A. Görling, *J. Chem. Phys.* **127**, 054102 (2007).

- [43] C. Kollmar and M. Filatov, *J. Chem. Phys.* **127**, 114104 (2007).
- [44] J. Fernandez, C. Kollmar, and M. Filatov, *Phys. Rev. A* **82**, 16 (2010).
- [45] F. Bulat, T. Heaton-Burgess, A. J. Cohen, and W. Yang, *J. Chem. Phys.* **127**, 174101 (2007).
- [46] Ch. R. Jacob, *J. Chem. Phys.* **135**, 244102 (2011).
- [47] O. V. Gritsenko and E. J. Baerends, *J. Chem. Phys.* **120**, 8364 (2004).
- [48] U. von Barth and L. Hedin, *J. Phys. C* **5**, 1629 (1972).
- [49] Ch. R. Jacob and M. Reiher, *Int. J. Quantum Chem.* **112**, 3661 (2012).
- [50] J. A. Pople, P. M. W. Gill, and N. C. Handy, *Int. J. Quantum Chem.* **56**, 303 (1995).
- [51] J. P. Perdew, A. Ruzsinszky, L. A. Constantin, J. Sun, and G. I. Csonka, *J. Chem. Theory Comput.* **5**, 902 (2009).
- [52] Y. Wang and R. G. Parr, *Phys. Rev. A* **47**, R1591 (1993).
- [53] Q. Zhao, R. C. Morrison, and R. G. Parr, *Phys. Rev. A* **50**, 2138 (1994).
- [54] F. Colonna and A. Savin, *J. Chem. Phys.* **110**, 2828 (1999).
- [55] E. S. Kadantsev and M. J. Stott, *Phys. Rev. A* **69**, 012502 (2004).
- [56] O. V. Gritsenko, R. van Leeuwen, and E. J. Baerends, *Phys. Rev. A* **52**, 1870 (1995).
- [57] P. R. T. Schipper, O. V. Gritsenko, and E. J. Baerends, *Theor. Chem. Acc.* **99**, 329 (1998).
- [58] S. Hirata, S. Ivanov, I. Grabowski, R. J. Bartlett, K. Burke, and J. D. Talman, *J. Chem. Phys.* **115**, 1635 (2001).
- [59] G. L. Oliver and J. P. Perdew, *Phys. Rev. A* **20**, 397 (1979).

- [60] M. Levy, Proc. Natl. Acad. Sci. **76**, 6062 (1979).
- [61] M. Levy, Phys. Rev. A **26**, 1200 (1982).
- [62] T. Heaton-Burgess and W. Yang, J. Chem. Phys. **129**, 194102 (2008).
- [63] G. te Velde, F. M. Bickelhaupt, E. J. Baerends, C. Fonseca Guerra, S. J. A. van Gisbergen, J. G. Snijders, and T. Ziegler, J. Comput. Chem. **22**, 931 (2001), see <http://www.scm.com>.
- [64] Ch. R. Jacob, S. M. Beyhan, R. E. Bulo, A. S. P. Gomes, A. W. Götz, K. Kiewisch, J. Sikkema, and L. Visscher, J. Comput. Chem. **32**, 2328 (2011).
- [65] Q. Wu and W. Yang, J. Theo. Comp. Chem. **2**, 627 (2003).
- [66] A. N. Tihonov, Dokl. Akad. Nauk SSSR **151**, 501 (1963).
- [67] W. H. Press, A. A. Teukolsky, W. T. Vetterling, and B. P. Flannery, *Numerical Recipes: The Art of Scientific Computing*, Cambridge University Press, 3rd edition, 2007.
- [68] M. J. G. Peach, D. G. J. Griffiths, and D. J. Tozer, J. Chem. Phys. **136**, 144101 (2012).
- [69] P. de Silva and T. A. Wesolowski, Phys. Rev. A **85**, 032518 (2012).
- [70] D. Andrae and J. Hinze, Int. J. Quantum Chem. **63**, 65 (1997).
- [71] G. Eickerling and M. Reiher, J. Chem. Theory Comput. **4**, 286 (2008).
- [72] H.-J. Werner et al., Molpro, version 2009.1, a package of *ab initio* programs, 2009, see <http://www.molpro.net>.
- [73] T. H. Dunning, Jr., J. Chem. Phys. **90**, 1007 (1989).
- [74] N. B. Balabanov and K. A. Peterson, J. Chem. Phys. **123**, 064107 (2005).
- [75] P. R. T. Schipper, O. V. Gritsenko, and E. J. Baerends, Theor. Chem. Acc. **98**, 16 (1997).

List of Figures

- 1 Target radial (a) total densities and (b) spin densities for the lithium atom obtained from BP86/QZ4P and Full-CI/cc-pVTZ calculations. The difference between these two target densities is shown in the lower part. The insets present the difference between the target total and spin densities and the corresponding density obtained in the finite orbital basis set from the Wu–Yang optimized potentials (upper insets) and from the optimal optimized potentials (lower insets). For the Full-CI/cc-pVTZ results obtained with both the TZ2P and QZ4P orbital basis sets in the potential reconstruction are included. The corresponding plots of the α - and β -electron densities are given in Fig. 1 in the Supporting Information. 42

- 2 Reconstructed potentials determined for the Li atom and a BP86/QZ4P target (spin) density. The upper part shows the exchange–correlation potentials for (a) α electrons v_{xc}^α and (b) β electrons v_{xc}^β , while the lower part shows (c) the total exchange–correlation potential v_{xc}^{tot} and (d) the spin exchange–correlation potential v_{xc}^{spin} . For the potential reconstruction with the finite QZ4P orbital basis set, the potentials obtained with the different schemes for singling out an unambiguous potential (see text for details) are shown. The accurate potentials obtained with a numerical solution of the KS equations (“*numerical (STO)*”) as well as the BP86 exchange–correlation potential calculated from the reference density (“*BP86 xc potential*”) are shown for comparison. The latter is shifted such that it agrees with the numerical reference at $r = 5$ bohr. 43

- 3 Reconstructed potentials determined for the Li atom and a Full-CI/cc-pVTZ target (spin) density with a TZ2P and with a QZ4P orbital basis set in the potential reconstruction. The upper part shows the (a) total exchange–correlation potentials v_{xc}^{tot} and (b) the spin exchange–correlation potentials v_{xc}^{spin} obtained with the TZ2P orbital basis set in the potential reconstruction, whereas the lower part (c) and (d) shows the corresponding results for the QZ4P orbital basis set. The accurate potentials obtained with a numerical solution of the KS equations (“*numerical (GTO)*”) from the GTO target density as well as from the Wu–Yang reconstructed density (“*numerical (STO)*”) are shown for comparison. These reference potentials have been shifted such that they agree with the optimal potential at $r = 2.7$ bohr. The corresponding plots of the α - and β -electron potentials are given in Fig. 2 in the Supporting Information. 44
- 4 Target spin densities for the dioxygen molecule obtained from BP86/QZ4P and CAS(12,12)SCF/cc-pVTZ calculations. Both spin densities are compared (a) along the bond axis (x -axis), (b) perpendicular to the bond axis (y -axis). Furthermore, (c) and (d) show the BP86/QZ4P and CAS(12,12)SCF/cc-pVTZ spin densities, respectively, in the xy -plane. The corresponding plots of the total and the individual α - and β -electron densities are given in Fig. 6 in the Supporting Information. 45
- 5 Reconstructed potentials determined for the dioxygen molecule and a BP86/QZ4P target (spin) density. The upper part shows the total exchange–correlation potential v_{xc}^{tot} (a) along the bond axis (x axis) and (b) perpendicular to the bond axis along the y axis. The lower part shows the spin exchange–correlation potential v_{xc}^{spin} along the (c) x axis and (d) y axis. In the potential reconstruction, the finite QZ4P orbital basis set was employed. For comparison, the BP86 exchange–correlation potential calculated from the reference density (“*BP86 xc potential*”) is also included. This BP86 potential is shifted such that it agrees with the optimal potential at $x = -2$ bohr or at $y = +2$ bohr, respectively. The corresponding plots of the individual α - and β -electron potentials are shown in Fig. 7 in the Supporting Information. 46

- 6 (a) Reconstructed spin exchange–correlation potential v_{xc}^{spin} determined for the dioxygen molecule and a BP86/QZ4P target (spin) density in the xy -plane. Here, only the optimal potential reconstructed within a QZ4P orbital basis set is included. For comparison, (b) shows the BP86 exchange–correlation potential calculated from the target density. 47
- 7 Reconstructed potentials determined for the dioxygen molecule and a CAS(12,12)SCF/cc-pVTZ target (spin) density. The upper part shows the total exchange–correlation potential v_{xc}^{tot} (a) along the bond axis (x axis) and (b) perpendicular to the bond axis along the y axis. The lower part shows the spin exchange–correlation potential v_{xc}^{spin} along the (c) x axis and (d) y axis. In the potential reconstruction, the finite QZ4P orbital basis set was employed. The corresponding plots of the individual α - and β -electron potentials as well as the results obtained with the TZ2P orbital basis set are shown in Fig. 8 and Figs. 10 and 11 in the Supporting Information, respectively. 48
- 8 Reconstructed spin exchange–correlation potential potentials determined for the dioxygen molecule and a CAS(12,12)SCF/cc-pVTZ target (spin) density. For the potential reconstruction with the finite QZ4P orbital basis set (a) the optimal spin potential and (b) the spin potential determined by requiring that the optimized potential is smooth are shown. The spin potential obtained by implicitly balancing the orbital and potential basis sets as well as the results obtained with the TZ2P orbital basis set are shown in Fig. 9 and Figs 12 and 13 in the Supporting Information, respectively. 49

Figure 1: Target radial (a) total densities and (b) spin densities for the lithium atom obtained from BP86/QZ4P and Full-CI/cc-pVTZ calculations. The difference between these two target densities is shown in the lower part. The insets present the difference between the target total and spin densities and the corresponding density obtained in the finite orbital basis set from the Wu–Yang optimized potentials (upper insets) and from the optimal optimized potentials (lower insets). For the Full-CI/cc-pVTZ results obtained with both the TZ2P and QZ4P orbital basis sets in the potential reconstruction are included. The corresponding plots of the α - and β -electron densities are given in Fig. 1 in the Supporting Information.

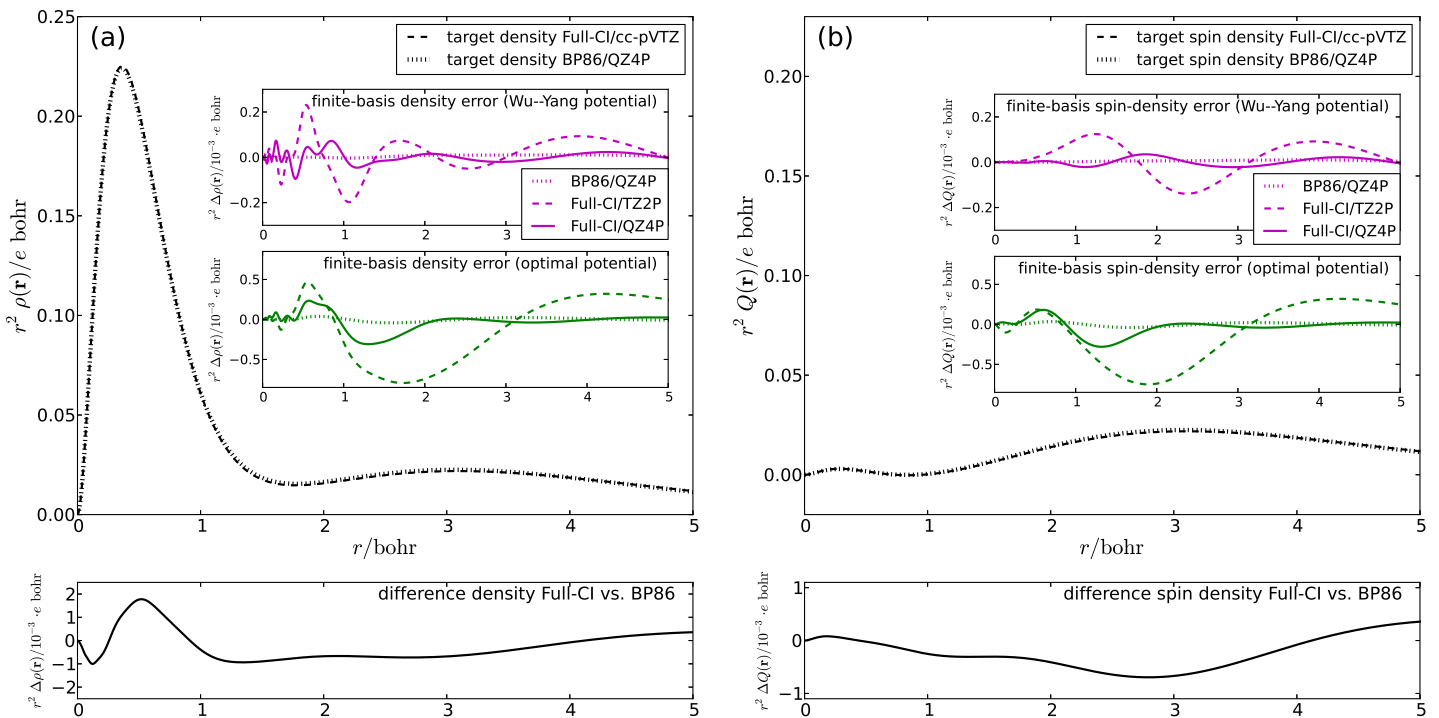


Figure 2: Reconstructed potentials determined for the Li atom and a BP86/QZ4P target (spin) density. The upper part shows the exchange–correlation potentials for (a) α electrons v_{xc}^α and (b) β electrons v_{xc}^β , while the lower part shows (c) the total exchange–correlation potential v_{xc}^{tot} and (d) the spin exchange–correlation potential v_{xc}^{spin} . For the potential reconstruction with the finite QZ4P orbital basis set, the potentials obtained with the different schemes for singling out an unambiguous potential (see text for details) are shown. The accurate potentials obtained with a numerical solution of the KS equations (“*numerical (STO)*”) as well as the BP86 exchange–correlation potential calculated from the reference density (“*BP86 xc potential*”) are shown for comparison. The latter is shifted such that it agrees with the numerical reference at $r = 5$ bohr.

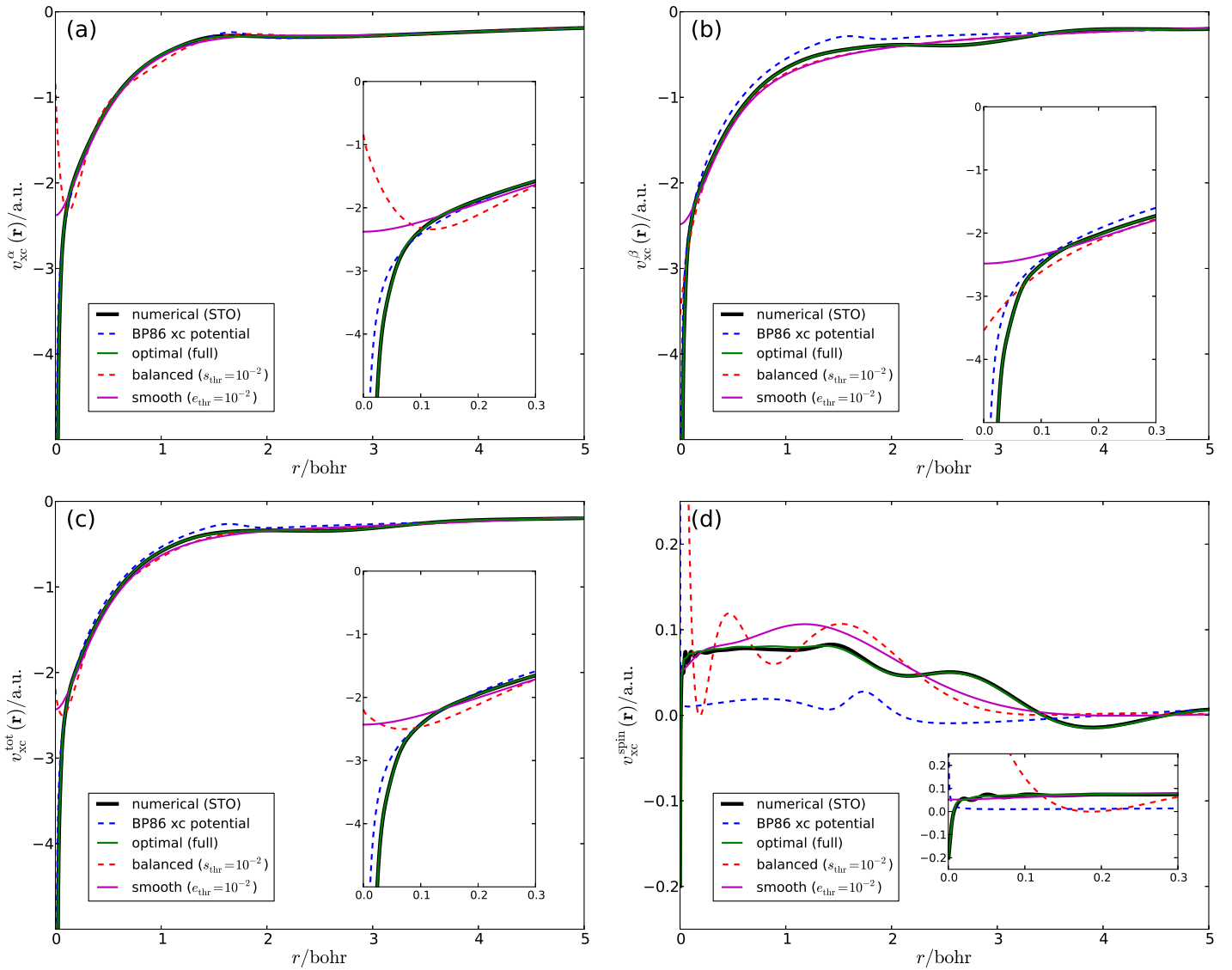


Figure 3: Reconstructed potentials determined for the Li atom and a Full-CI/cc-pVTZ target (spin) density with a TZ2P and with a QZ4P orbital basis set in the potential reconstruction. The upper part shows the (a) total exchange–correlation potentials v_{xc}^{tot} and (b) the spin exchange–correlation potentials v_{xc}^{spin} obtained with the TZ2P orbital basis set in the potential reconstruction, whereas the lower part (c) and (d) shows the corresponding results for the QZ4P orbital basis set. The accurate potentials obtained with a numerical solution of the KS equations (“numerical (GTO)”) from the GTO target density as well as from the Wu–Yang reconstructed density (“numerical (STO)”) are shown for comparison. These reference potentials have been shifted such that they agree with the optimal potential at $r = 2.7$ bohr. The corresponding plots of the α - and β -electron potentials are given in Fig. 2 in the Supporting Information.

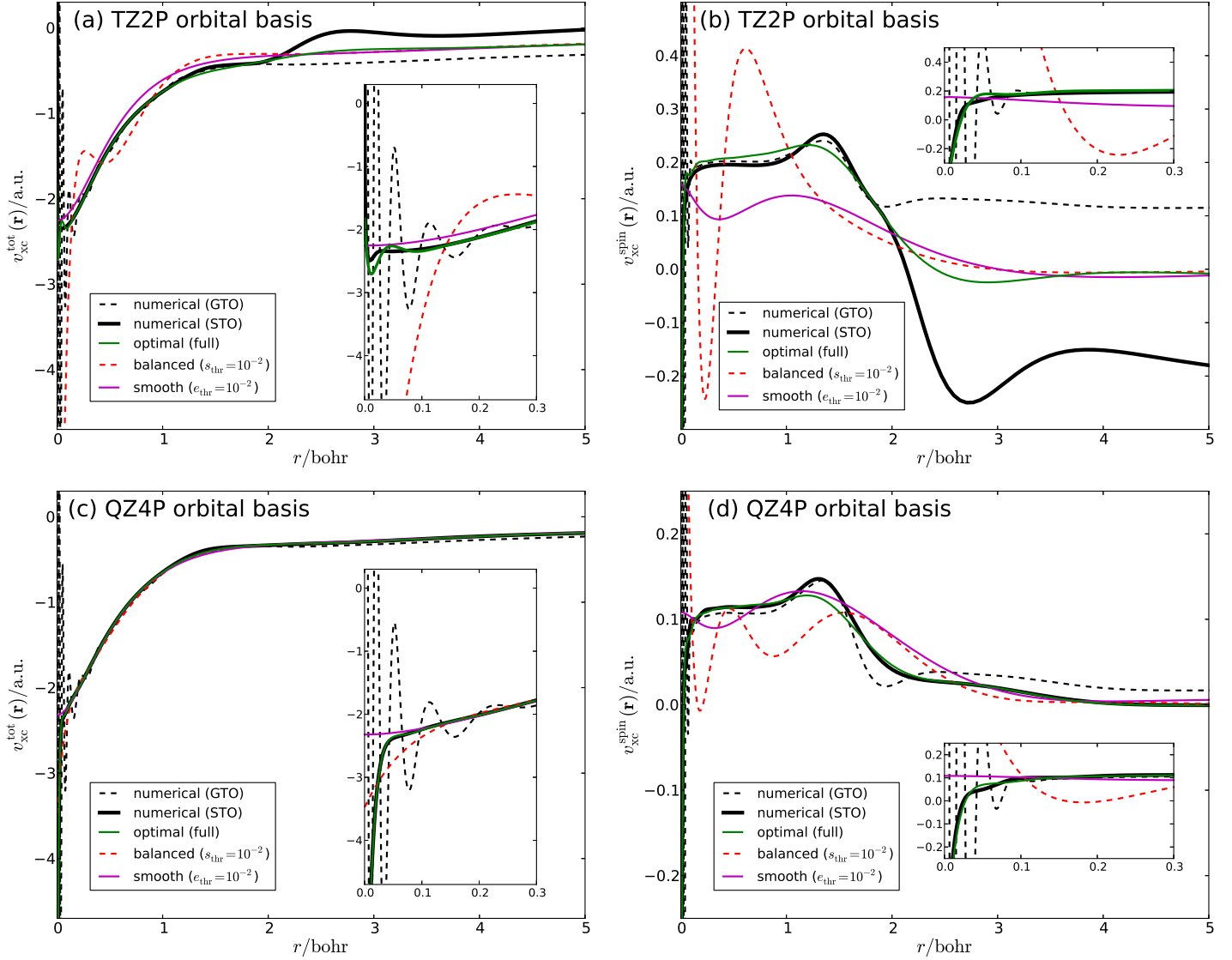


Figure 4: Target spin densities for the dioxygen molecule obtained from BP86/QZ4P and CAS(12,12)SCF/cc-pVTZ calculations. Both spin densities are compared (a) along the bond axis (x -axis), (b) perpendicular to the bond axis (y -axis). Furthermore, (c) and (d) show the BP86/QZ4P and CAS(12,12)SCF/cc-pVTZ spin densities, respectively, in the xy -plane. The corresponding plots of the total and the individual α - and β -electron densities are given in Fig. 6 in the Supporting Information.

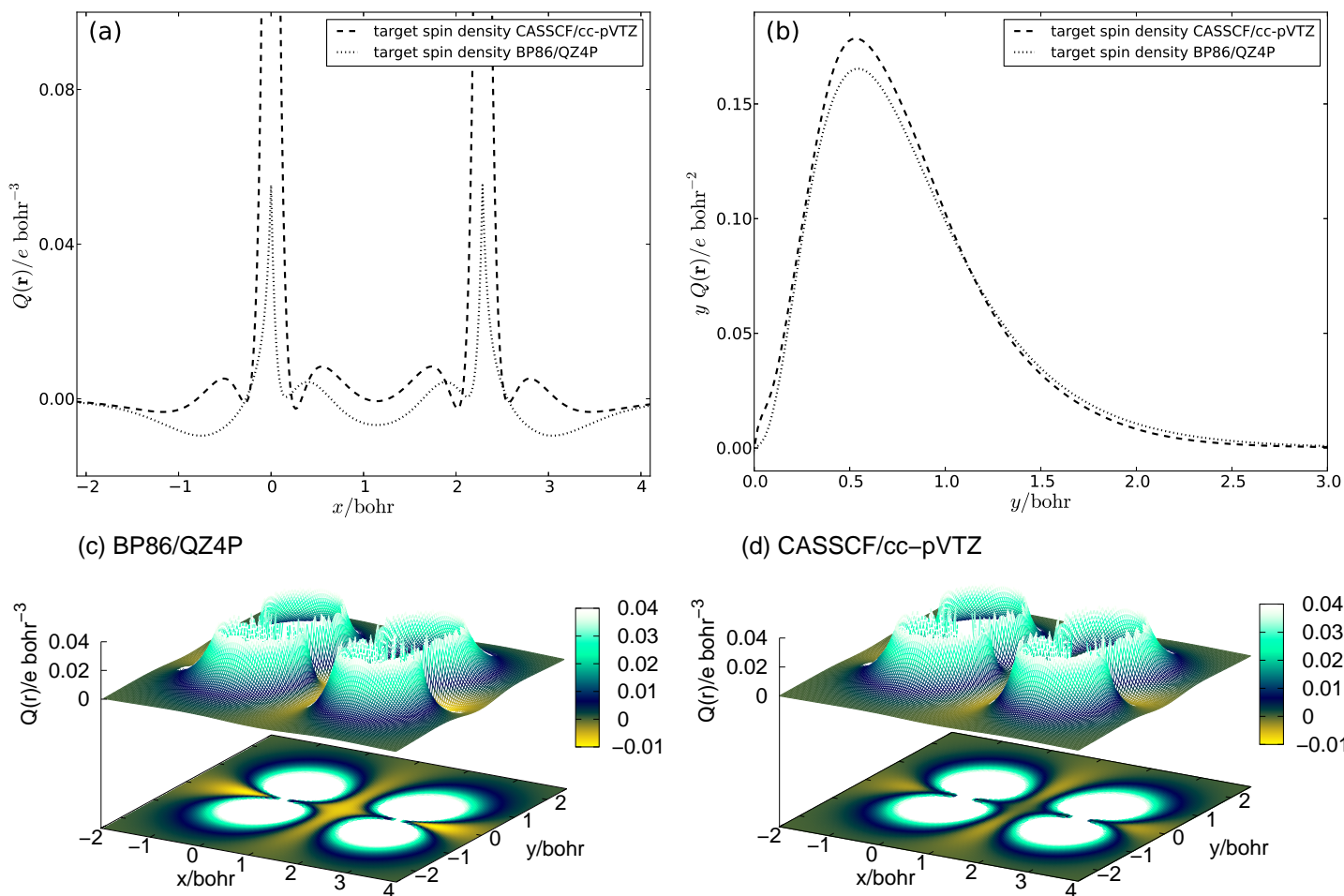


Figure 5: Reconstructed potentials determined for the dioxygen molecule and a BP86/QZ4P target (spin) density. The upper part shows the total exchange–correlation potential v_{xc}^{tot} (a) along the bond axis (x axis) and (b) perpendicular to the bond axis along the y axis. The lower part shows the spin exchange–correlation potential v_{xc}^{spin} along the (c) x axis and (d) y axis. In the potential reconstruction, the finite QZ4P orbital basis set was employed. For comparison, the BP86 exchange–correlation potential calculated from the reference density (“BP86 xc potential”) is also included. This BP86 potential is shifted such that it agrees with the optimal potential at $x = -2$ bohr or at $y = +2$ bohr, respectively. The corresponding plots of the individual α - and β -electron potentials are shown in Fig. 7 in the Supporting Information.

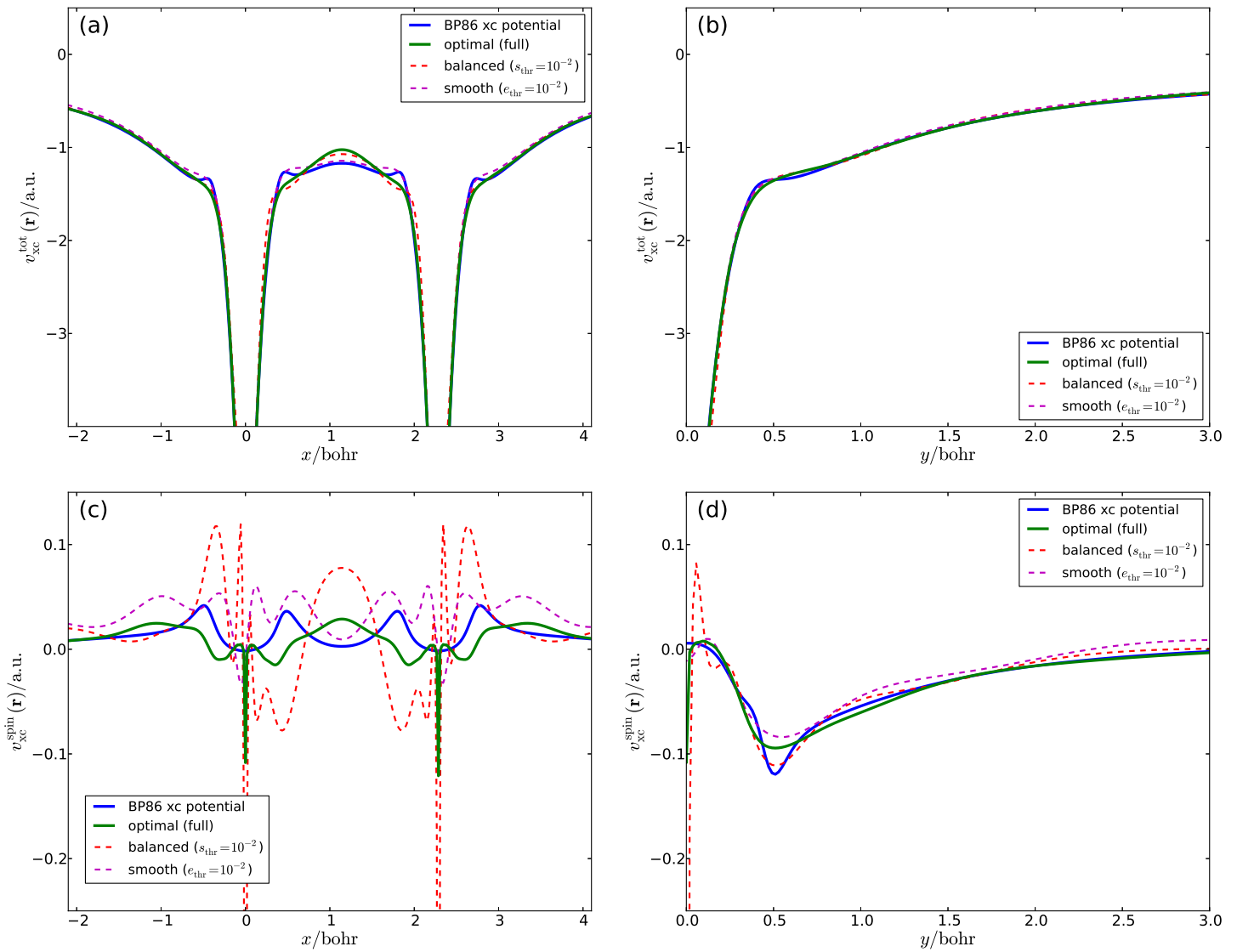


Figure 6: (a) Reconstructed spin exchange–correlation potential v_{xc}^{spin} determined for the dioxygen molecule and a BP86/QZ4P target (spin) density in the xy -plane. Here, only the optimal potential reconstructed within a QZ4P orbital basis set is included. For comparison, (b) shows the BP86 exchange–correlation potential calculated from the target density.

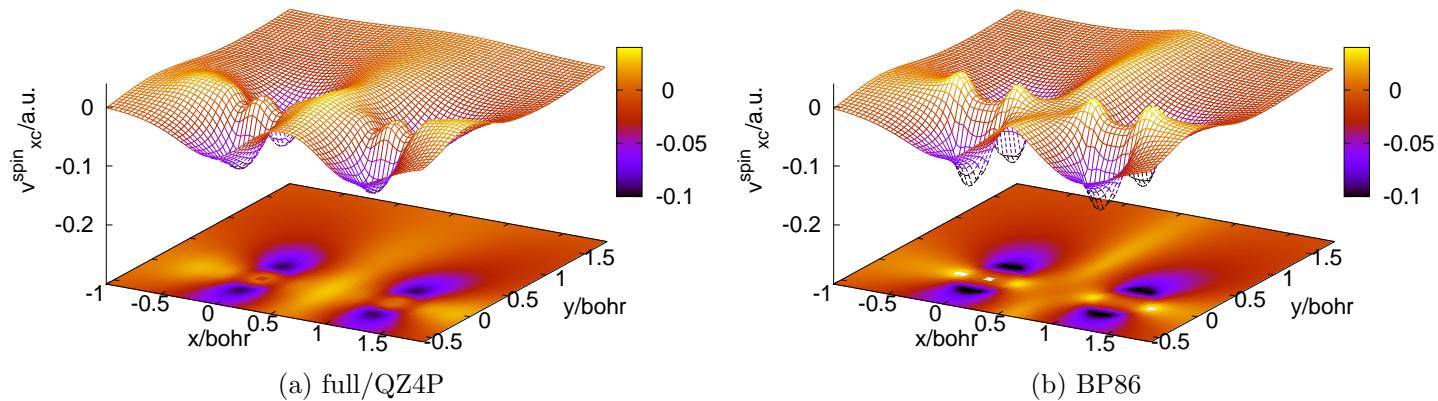


Figure 7: Reconstructed potentials determined for the dioxygen molecule and a CAS(12,12)SCF/cc-pVTZ target (spin) density. The upper part shows the total exchange–correlation potential v_{xc}^{tot} (a) along the bond axis (x axis) and (b) perpendicular to the bond axis along the y axis. The lower part shows the spin exchange–correlation potential v_{xc}^{spin} along the (c) x axis and (d) y axis. In the potential reconstruction, the finite QZ4P orbital basis set was employed. The corresponding plots of the individual α - and β -electron potentials as well as the results obtained with the TZ2P orbital basis set are shown in Fig. 8 and Figs. 10 and 11 in the Supporting Information, respectively.

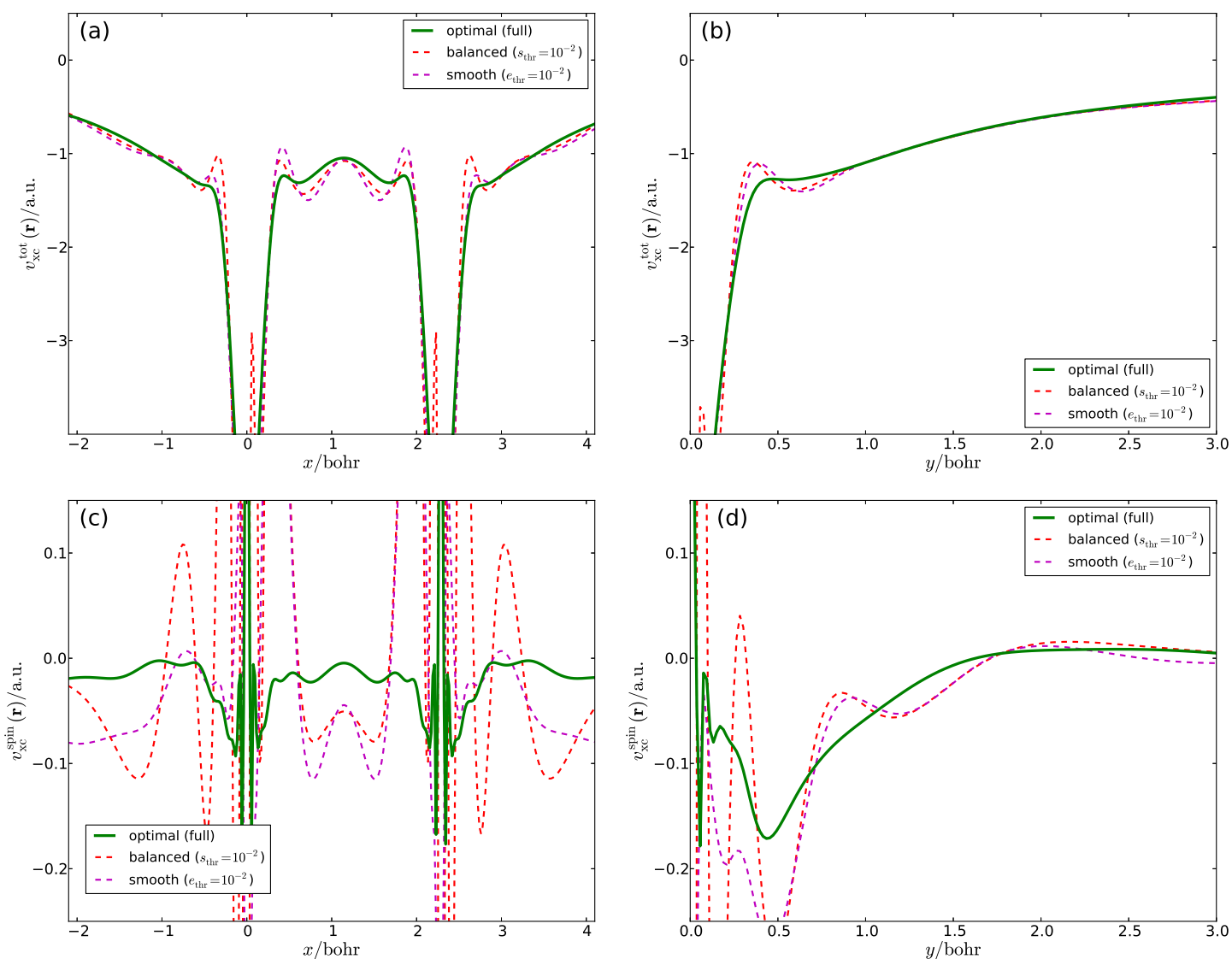
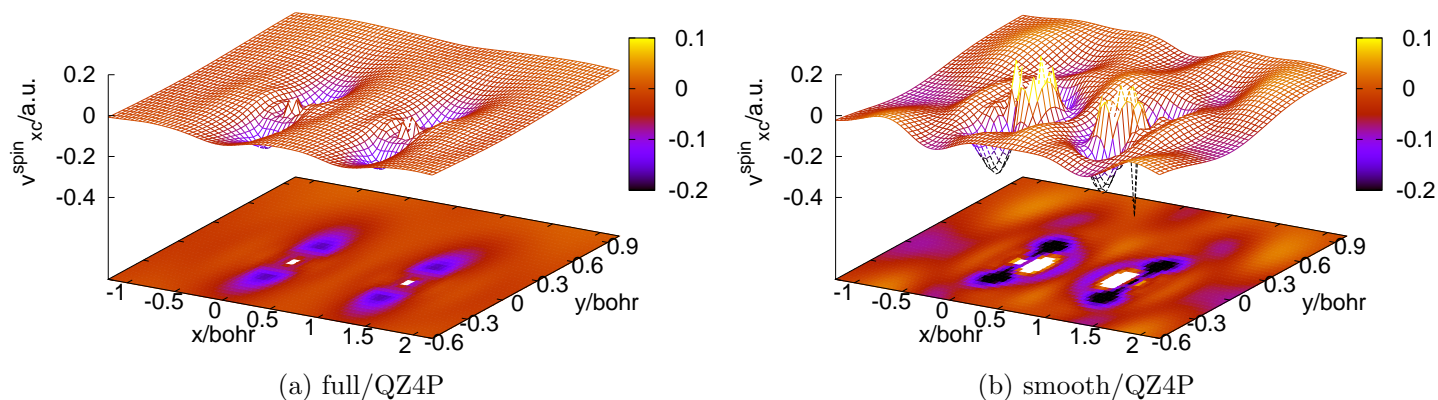


Figure 8: Reconstructed spin exchange–correlation potential potentials determined for the dioxygen molecule and a CAS(12,12)SCF/cc-pVTZ target (spin) density. For the potential reconstruction with the finite QZ4P orbital basis set (a) the optimal spin potential and (b) the spin potential determined by requiring that the optimized potential is smooth are shown. The spin potential obtained by implicitly balancing the orbital and potential basis sets as well as the results obtained with the TZ2P orbital basis set are shown in Fig. 9 and Figs 12 and 13 in the Supporting Information, respectively.



List of Tables

| | | |
|-----|---|----|
| I | Absolute errors $\Delta_{\text{abs}}^{\sigma}$ in the α - and β -electron densities with respect to the target α - and β -electron densities (in e bohr ⁻³) obtained with different reconstructed potentials for the Li atom with BP86/QZ4P target densities. The QZ4P orbital basis set is used in the finite-basis set potential reconstruction. $\Delta_{\text{abs}}^{\sigma,\text{finite}}$ refers to the error in the density obtained from the respective potentials in the finite orbital basis set, whereas $\Delta_{\text{abs}}^{\sigma,\text{num}}$ is the error for the density obtained from a numerical solution of the KS equations. | 51 |
| II | Absolute errors $\Delta_{\text{abs}}^{\sigma}$ in the α - and β -electron densities with respect to the target α - and β -electron densities (in e bohr ⁻³) obtained with different reconstructed potentials for the Li atom and Full-CI/cc-pVTZ target densities. Results obtained both with the TZ2P and with the QZ4P orbital basis set in the potential reconstruction are shown. $\Delta_{\text{abs}}^{\sigma,\text{finite}}$ refers to the error in the density obtained from the respective potentials in the finite orbital basis set, whereas $\Delta_{\text{abs}}^{\sigma,\text{num}}$ is the error for the density obtained from a numerical solution of the KS equations. | 52 |
| III | Absolute errors $\Delta_{\text{abs}}^{\sigma,\text{finite}}$ in the α - and β -electron densities in the finite orbital basis set with respect to the target α - and β -electron densities (in e bohr ⁻³) obtained with different reconstructed potentials for the dioxygen molecule. Results are shown for both the target densities from BP86 and from a CAS(12,12)SCF calculation and in the latter case using both the TZ2P and with the QZ4P orbital basis set in the potential reconstruction. | 53 |

Table I: Absolute errors $\Delta_{\text{abs}}^{\sigma}$ in the α - and β -electron densities with respect to the target α - and β -electron densities (in e bohr $^{-3}$) obtained with different reconstructed potentials for the Li atom with BP86/QZ4P target densities. The QZ4P orbital basis set is used in the finite-basis set potential reconstruction. $\Delta_{\text{abs}}^{\sigma,\text{finite}}$ refers to the error in the density obtained from the respective potentials in the finite orbital basis set, whereas $\Delta_{\text{abs}}^{\sigma,\text{num}}$ is the error for the density obtained from a numerical solution of the KS equations.

| | $\Delta_{\text{abs}}^{\alpha,\text{num}}$ | $\Delta_{\text{abs}}^{\alpha,\text{finite}}$ | $\Delta_{\text{abs}}^{\beta,\text{num}}$ | $\Delta_{\text{abs}}^{\beta,\text{finite}}$ |
|---|---|--|--|---|
| Numerical (STO) | $< 10^{-4}$ | 0.0007 | $< 10^{-4}$ | 0.0001 |
| Wu–Yang | 0.0098 | 0.0008 | 0.0036 | $< 10^{-4}$ |
| Balanced ($s_{\text{thr}} = 10^{-2}$) | 0.0090 | 0.0024 | 0.0016 | 0.0006 |
| Smooth ($e_{\text{thr}} = 10^{-2}$) | 0.0087 | 0.0086 | 0.0082 | 0.0082 |
| Optimal (full) | 0.0009 | 0.0014 | $< 10^{-4}$ | $< 10^{-4}$ |

Table II: Absolute errors $\Delta_{\text{abs}}^{\sigma}$ in the α - and β -electron densities with respect to the target α - and β -electron densities (in e bohr⁻³) obtained with different reconstructed potentials for the Li atom and Full-CI/cc-pVTZ target densities. Results obtained both with the TZ2P and with the QZ4P orbital basis set in the potential reconstruction are shown. $\Delta_{\text{abs}}^{\sigma,\text{finite}}$ refers to the error in the density obtained from the respective potentials in the finite orbital basis set, whereas $\Delta_{\text{abs}}^{\sigma,\text{num}}$ is the error for the density obtained from a numerical solution of the KS equations.

| Full-CI/cc-pVTZ | TZ2P | | | | QZ4P | | | |
|---|---|--|--|---|---|--|--|---|
| | $\Delta_{\text{abs}}^{\alpha,\text{num}}$ | $\Delta_{\text{abs}}^{\alpha,\text{finite}}$ | $\Delta_{\text{abs}}^{\beta,\text{num}}$ | $\Delta_{\text{abs}}^{\beta,\text{finite}}$ | $\Delta_{\text{abs}}^{\alpha,\text{num}}$ | $\Delta_{\text{abs}}^{\alpha,\text{finite}}$ | $\Delta_{\text{abs}}^{\beta,\text{num}}$ | $\Delta_{\text{abs}}^{\beta,\text{finite}}$ |
| Numerical (GTO) | $< 10^{-4}$ | 0.0258 | $< 10^{-4}$ | 0.0086 | $< 10^{-4}$ | 0.0065 | $< 10^{-4}$ | 0.0010 |
| Numerical (STO) | 0.0051 | 0.0158 | 0.0020 | 0.0014 | 0.0025 | 0.0051 | 0.0005 | 0.0005 |
| Wu–Yang | 0.0782 | 0.0051 | 0.0301 | 0.0020 | 0.0165 | 0.0025 | 0.0021 | 0.0004 |
| Balanced ($s_{\text{thr}} = 10^{-2}$) | 0.0336 | 0.0079 | 0.0310 | 0.0020 | 0.0092 | 0.0074 | 0.0030 | 0.0004 |
| Smooth ($e_{\text{thr}} = 10^{-2}$) | 0.0416 | 0.0105 | 0.0039 | 0.0041 | 0.0120 | 0.0071 | 0.0062 | 0.0061 |
| Optimal (full) | 0.0220 | 0.0284 | 0.0021 | 0.0016 | 0.0061 | 0.0067 | 0.0005 | 0.0006 |

Table III: Absolute errors $\Delta_{\text{abs}}^{\sigma, \text{finite}}$ in the α - and β -electron densities in the finite orbital basis set with respect to the target α - and β -electron densities (in e bohr⁻³) obtained with different reconstructed potentials for the dioxygen molecule. Results are shown for both the target densities from BP86 and from a CAS(12,12)SCF calculation and in the latter case using both the TZ2P and with the QZ4P orbital basis set in the potential reconstruction.

| | BP86/QZ4P | | CASSCF/TZ2P | | CASSCF/QZ4P | |
|---|---|--|---|--|---|--|
| | $\Delta_{\text{abs}}^{\alpha, \text{finite}}$ | $\Delta_{\text{abs}}^{\beta, \text{finite}}$ | $\Delta_{\text{abs}}^{\alpha, \text{finite}}$ | $\Delta_{\text{abs}}^{\beta, \text{finite}}$ | $\Delta_{\text{abs}}^{\alpha, \text{finite}}$ | $\Delta_{\text{abs}}^{\beta, \text{finite}}$ |
| Wu–Yang | 0.0002 | 0.0002 | 0.0419 | 0.0439 | 0.0412 | 0.0268 |
| Balanced ($s_{\text{thr}} = 10^{-2}$) | 0.0019 | 0.0010 | 0.0521 | 0.0537 | 0.0414 | 0.0278 |
| Smooth ($e_{\text{thr}} = 10^{-2}$) | 0.0077 | 0.0078 | 0.0426 | 0.0462 | 0.0416 | 0.0277 |
| Optimal (full) | 0.0284 | 0.0230 | 0.0976 | 0.0830 | 0.0640 | 0.0509 |